

This is a repository copy of *A Direct Fluorescent Activity Assay for Glycosyltransferases Enables Convenient High-Throughput Screening:Application to O-GlcNAc Transferase*.

White Rose Research Online URL for this paper:

<https://eprints.whiterose.ac.uk/159729/>

Version: Accepted Version

---

**Article:**

Alteen, Matthew G., Gros, Christina, Meek, Richard W. et al. (11 more authors) (2020) A Direct Fluorescent Activity Assay for Glycosyltransferases Enables Convenient High-Throughput Screening:Application to O-GlcNAc Transferase. *Angewandte Chemie International Edition*. pp. 9601-9609. ISSN 1433-7851

<https://doi.org/10.1002/ange.202000621>

---

**Reuse**

Items deposited in White Rose Research Online are protected by copyright, with all rights reserved unless indicated otherwise. They may be downloaded and/or printed for private study, or other acts as permitted by national copyright laws. The publisher or other rights holders may allow further reproduction and re-use of the full text version. This is indicated by the licence information on the White Rose Research Online record for the item.

**Takedown**

If you consider content in White Rose Research Online to be in breach of UK law, please notify us by emailing [eprints@whiterose.ac.uk](mailto:eprints@whiterose.ac.uk) including the URL of the record and the reason for the withdrawal request.

# A direct fluorescent activity assay for glycosyltransferases enables convenient high-throughput screening: Application to O-GlcNAc Transferase

Matthew G. Alteen,<sup>[a]</sup> Christina Gros,<sup>[a]</sup> Richard W. Meek,<sup>[b]</sup> David A. Cardoso,<sup>[c]</sup> Jil A. Busmann,<sup>[d]</sup> Gontran Sangouard,<sup>[a]</sup> Matthew C. Deen,<sup>[a]</sup> Hong-Yee Tan,<sup>[a]</sup> David L. Shen,<sup>[d]</sup> Cecilia C. Russell,<sup>[e]</sup> Gideon J. Davies,<sup>[b]</sup> Phillip J. Robinson,<sup>[c]</sup> Adam McCluskey<sup>[e]</sup> and David J. Vocadlo<sup>\*[a],[d]</sup>

<sup>[a]</sup> Department of Chemistry, Simon Fraser University, Burnaby, BC, V5A 1S6, Canada

<sup>[b]</sup> York Structural Biology Laboratory, Department of Chemistry, University of York, York, YO10 5DD, UK

<sup>[c]</sup> Children's Medical Research Institute, The University of Sydney, Sydney, NSW, 2145, Australia

<sup>[d]</sup> Department of Molecular Biology and Biochemistry, Simon Fraser University, Burnaby, BC, V5A 1S6, Canada

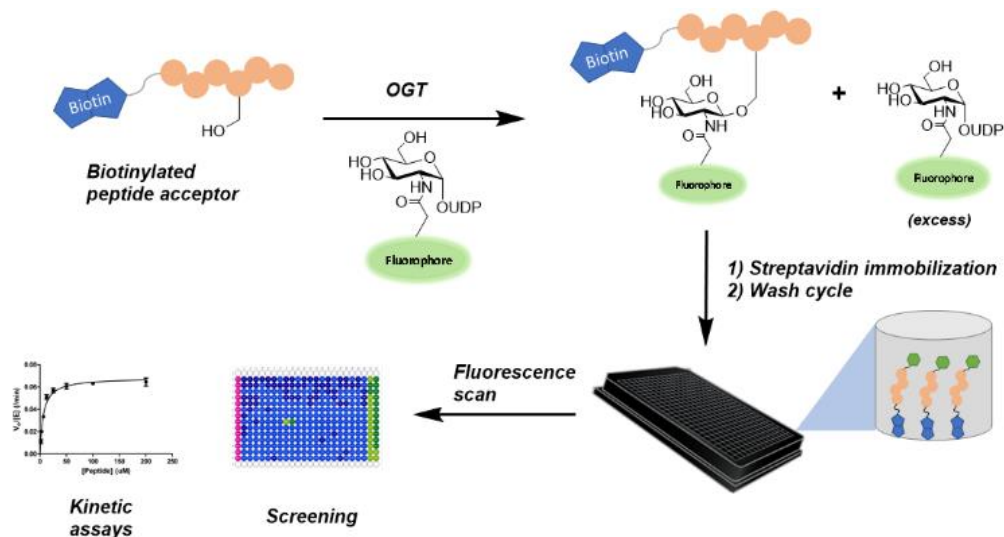
<sup>[e]</sup> Chemistry, School of Environmental and Life Sciences, The University of Newcastle, University Drive, Callaghan, NSW, 2308, Australia

\*Corresponding author: David J. Vocadlo ([dvocadlo@sfu.ca](mailto:dvocadlo@sfu.ca))

**Abstract:** Glycosyltransferases carry out important cellular functions in species ranging from bacteria to humans. Despite their essential roles in biology, simple and robust activity assays that can be easily applied to high-throughput screening for inhibitors of these enzymes have been challenging to develop. Here we report a bead-based strategy to sensitively measure the group transfer activity of glycosyltransferases using simple fluorescence measurements, without the need for coupled enzymes or secondary reactions. We validate the performance and accuracy of the assay using O-GlcNAc Transferase (OGT) as a model system through detailed Michaelis-Menten kinetic analysis of various substrates and inhibitors. Optimization of this assay and application to high-throughput screening enabled screening for inhibitors of OGT, leading to a novel inhibitory scaffold. We believe this assay will prove valuable not only for the study of OGT, but also more widely as a general approach for the screening of glycosyltransferases and other group transfer enzymes.

**Keywords:** Glycosyltransferase, enzyme assay, high-throughput screening, O-GlcNAc, glycoprotein, fluorescent substrates

## Table of contents figure



A robust fluorescence-based assay accurately reports on the sugar transfer activity of glycosyltransferases. This assay is amenable to high-throughput screening and should be applicable to a diverse set of group transfer enzymes. We validate this assay through screening of a library of known bioactive molecules to identify a new O-GlcNAc Transferase antagonist.

## **Introduction**

The large superfamily of glycosyltransferases (GTs) are responsible for the assembly of the diverse glycoconjugates found throughout every kingdom of life<sup>[1,2]</sup>. The increasing recognition of the roles played by glycans, including in regulating human physiology, are raising interest in these enzymes and the associated development of chemical approaches to monitor and modulate their activities<sup>[3-6]</sup>. One area of emerging interest is the development of reliable glycosyltransferase enzyme assays for characterizing their activities<sup>[7,8]</sup>, alongside with their use in high throughput screening efforts to identify small molecule inhibitors<sup>[4,9]</sup>. The standard activity assay that directly measures glycosyl transfer relies on the enzyme catalyzed transfer of radiolabeled sugar units from nucleotide sugar donor substrates to a suitable acceptor substrate, which is then followed by liquid scintillation detection<sup>[9-11]</sup>. The requirement for using radioactive materials, however, detracts from the wide uptake and applicability of such assays and has spurred interest in developing new assays for various GTs.

Among the various strategies that have been pursued are coupled enzyme activity assays that, for example, include measuring the release of nucleoside diphosphate leaving groups *via* spectrophotometric detection of reduced nicotinamide adenine dinucleotide (NADH) or the consumption of nucleoside diphosphates (NDPs) to drive formation of adenosine triphosphate (ATP) that is then detected by bioluminescence<sup>[12,13]</sup>. ELISA-based luminescent approaches have also been developed, whereby transfer of a monosaccharide unit is detected by a tagged pan-specific antibody<sup>[14]</sup>. Additionally, a coupled fucosyltransferase assay, in which transfer of a fucose to a fluorogenic oligosaccharide prevents a glycoside hydrolase from acting to release the fluorophore reporter was developed recently<sup>[15]</sup>. Various fluorescence polarization (FP) assays have also been advanced. Walker and colleagues, who pioneered work on screening for inhibitors of *O*-GlcNAc Transferase (OGT), used a fluorescein-linked UDP-GlcNAc analogue that served as a probe for an FP binding assay<sup>[16]</sup>. Paulson and colleagues expanded further on this approach by developing fluorescently-labeled nucleotide sugar donors that are substrates for a sialyl and fucosyltransferase, resulting in increased polarization when transferred to a glycoprotein substrate<sup>[4]</sup>. Withers and co-workers extended this approach to create an “FP-Tag” assay which uses an azide-labeled glycosyl donor that is transferred to a fluorescent oligosaccharide and conjugated to biotin *via* click chemistry, permitting pull-down with streptavidin and subsequent FP detection<sup>[17]</sup>.

While these methods represent notable advancements, the use of coupled assays requiring a secondary enzyme or chemical transfer step is not ideal as this introduces an

additional step at which test materials can interfere. In HTS assays in particular, such interference can yield a high number of false positives resulting from inhibition of the secondary processes instead of the primary target<sup>[18]</sup>. FP assays also do not directly measure enzymatic activity and compounds that disrupt binding through non-specific means, such as binding or displacing the fluorophore non-specifically from the surface of a protein, can similarly yield false positives<sup>[19,20]</sup>. Additionally, FP assays require high concentrations of protein and are sometimes incapable of detecting weak interactions<sup>[20]</sup>. Given these considerations, we aimed to develop a simple and direct quantitative fluorescence-based assay that would provide high-quality kinetic data using only small amounts of enzyme without the need for downstream coupling enzymes, bioorthogonal reactions, or detection reagents. This concept has been applied to binding processes, notably for fluorescently-labeled aptamers<sup>[21]</sup>, but surprisingly has never, to our knowledge, been applied to group transfer enzymes such as GTs. However, we expected that such an assay might prove useful for ongoing efforts to study the enzymatic activity of GTs toward various substrates as well as to characterize molecules that could modulate the activity of these enzymes. Moreover, we envisioned that adaptation of such an assay to a format compatible with high-throughput screening would facilitate identifying new leads for GTs that could be suitable for development as tool compounds.

As a model system of high interest with which we have experience, we focused on the enzyme *O*-GlcNAc Transferase (OGT), which catalyzes the installation of a single *O*-linked *N*-acetylglucosamine (*O*-GlcNAc) to the hydroxyl groups of serine and threonine residues of nuclear and cytosolic proteins<sup>[22][23]</sup>. This reversible modification has been identified on hundreds of protein substrates<sup>[24]</sup> and regulates central cellular processes such as transcription<sup>[25]</sup>, protein stability cellular stress response<sup>[26]</sup>, and cell cycle regulation<sup>[27]</sup>. Moreover, dysregulated OGT activity has been implicated in many signalling pathways related to cancer progression and tumor growth. Indeed, mounting evidence suggests that OGT is a promising therapeutic target for various cancers<sup>[28–31]</sup>. Furthermore, consistent with the high interest in this enzyme, previous efforts to screen OGT have been pursued and yielded various leads<sup>[16,32–34]</sup>. Improvement of these leads has, however, proven challenging. Walker and co-workers were the first to undertake this, carrying out two separate screens for OGT inhibitors using their FP displacement assay as well as a coupled protease protection assay<sup>[16,32]</sup>. These efforts resulted in a class of quinolone-6-sulfonate-based (Q6S) compounds,<sup>[33]</sup> which were recently advanced to yield promising compounds with nanomolar *in vitro* potency<sup>[34]</sup>. However, many of the inhibitors arising from these screens adversely affect cell viability and likely suffer from significant off-target effects<sup>[35]</sup>. Efforts to improve the potency of the Q6S scaffold over the past decade have yielded good success,

however, the resulting lead has a high molecular weight that may impair brain permeability and other *in vivo* applications. Ideally, as has often proven useful, the identification and advancement of new and diverse scaffolds that can be optimized are needed in order to ultimately identify complementary tool compounds for *in vivo* use.

Despite its importance in contributing to cellular physiology, and the complexity of the mechanisms by which OGT function must accordingly be regulated, studying this enzyme remains challenging in part because of a lack of convenient assays and chemical biology tools<sup>[14,36]</sup>. Here we describe the development of a simple and sensitive fluorescence-based assay that directly and precisely measures glycosyl transfer catalyzed by OGT. We validate this assay and illustrate its amenability to high-throughput screening in microplate format. After implementing the assay in a trial screen, we identify a known bioactive inhibitor that also antagonizes OGT and confirm its ability to directly inhibit OGT.

## ***Results and Discussion***

OGT is able to use uridine diphosphate *N*-acetylglucosamine (UDP-GlcNAc, **1**) analogues having various 2-*N*-acyl groups in place of the 2-acetamido substituent<sup>[16,37]</sup>. UDP-GlcNAc analogues bearing large fluorophores at this 2-position were previously found only to bind to OGT rather than be turned over<sup>[16]</sup>, however, judicious selection of linkers revealed appending a nitrobenzoxadiazole (NBD) fluorophore to this position was tolerated.<sup>[37]</sup> Based on these observations, we reasoned that using suitable linkers might enable incorporation of other fluorophores having different physicochemical and photophysical properties. We therefore elected to prepare a BODIPY-FL dye linked using an *N*-hexanoyl linker (**2**, UDP-GlcN-BODIPY, Figure 1). We were attracted to this option because of the relatively small size of this fluorophore in combination with its desirable photophysical properties, including high photostability and quantum yield. We therefore prepared UDP-GlcN-BODIPY (Scheme 1) by modification of established methods starting with glucosamine hydrochloride (**3**). After protection of the hydroxyl groups and masking of the amine as an azide functionality, we installed the anomeric phosphate using MacDonal phosphorylation conditions<sup>[38]</sup>. The acetate protecting groups were then removed, the azide reduced, and the resulting amine coupled to BODIPY-FL caproic acid using HBTU peptide coupling conditions. Finally, the desired nucleoside, UDP-GlcN-BODIPY, was prepared by coupling of intermediate **8** with UMP-morpholidate. We found after exploration of several routes that installation of the fluorophore prior to the morpholidate coupling permitted facile purification by silica chromatography and enabled suitable scale-up of this reaction. Details

regarding the synthesis, including preparation of BODIPY-FL caproic acid, are included in the Supporting Information (SI).

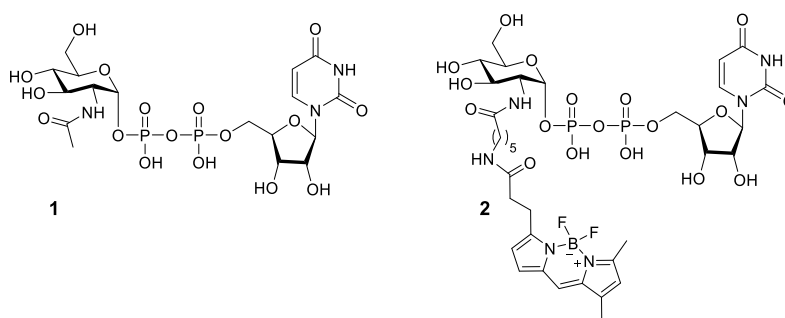
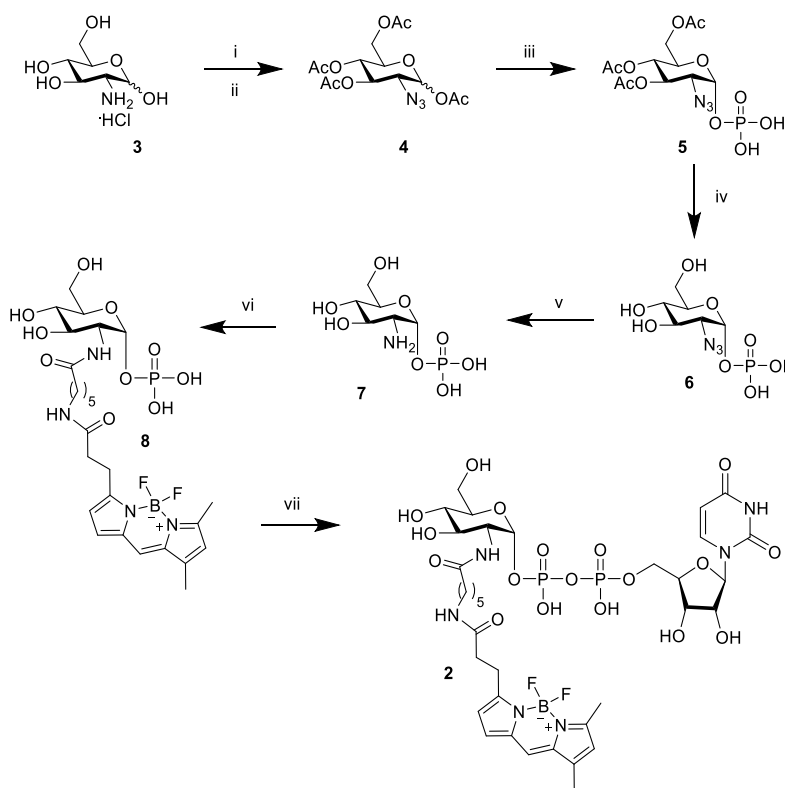


**Figure 1:** Structure of UDP-GlcNAc (**1**), the natural donor substrate used by OGT, and the fluorescent analogue UDP-GlcN-BODIPY (**2**).



**Scheme 1:** Synthetic route towards UDP-GlcN-BODIPY (**2**). Reagents and conditions: i) imidazole-1-sulfonyl azide•HCl,  $\text{CuSO}_4 \cdot 5\text{H}_2\text{O}$ ,  $\text{K}_2\text{CO}_3$ , MeOH, 2 h, 92%; ii)  $\text{Ac}_2\text{O}$ , pyridine, 10 h, 98%; iii)  $\text{H}_3\text{PO}_4$  (s), vacuum, 80 mTorr,  $60^\circ\text{C}$ , 44%; iv) NaOMe, MeOH, 92%; v)  $\text{H}_2$ , Pd/C, MeOH, 98%; vi) BODIPY-FL-X, HBTU, DIPEA, DMF, 37%; vii) UMP-morpholidate, N-methylimidazole•HCl, DMF, 45%.



With UDP-GlcN-BODIPY (**2**) in hand, we assessed its competency as a donor substrate for OGT using a well studied OGT peptide substrate derived from Casein Kinase II (CKII). Using this TAMRA-conjugated CKII peptide (TAMRA-NH-YPGGSTPVSSANMM-OH) we observed, using HPLC-based analysis, a modest level of transfer of the GlcN-BODIPY moiety to the peptide that was confirmed by mass spectrometry (MS) analysis of the reaction products (Figure S1). To understand the basis for molecular recognition of UDP-GlcN-BODIPY by OGT and how this enzyme tolerated this larger BODIPY moiety, we crystallized a truncated construct of OGT in complex with substrate UDP-GlcN-BODIPY<sup>[39]</sup>. This data (Table S1) enabled building a clear model revealing how the caproic acid linker is sufficiently long for the BODIPY fluorophore to completely extrude from the active site, causing minimal disruption of the active site architecture (Figure 2, Figure S2). Strong difference density was observable at the end of the linker and this is likely attributable to the BODIPY fluorophore, however, the fluorophore cannot be modelled with confidence (Figure S3). This ambiguity is likely a result of the BODIPY fluorophore occupying multiple conformations. A second BODIPY fluorophore can be modelled near the substrate (Figure 2), but this may stem from OGT-catalyzed hydrolysis of UDP-GlcN-BODIPY or, alternatively, a second molecule of substrate being present in proximity to the active site. The uridine and pyranose ring are positioned within the active site in a manner similar to those structures previously reported with bound UDP, except that there is a slight rotation in the  $\alpha$ -phosphate. This may stem from the altered position of Q839 leading to rotation of the  $\alpha$ -phosphate to within hydrogen bonding distance of T921.

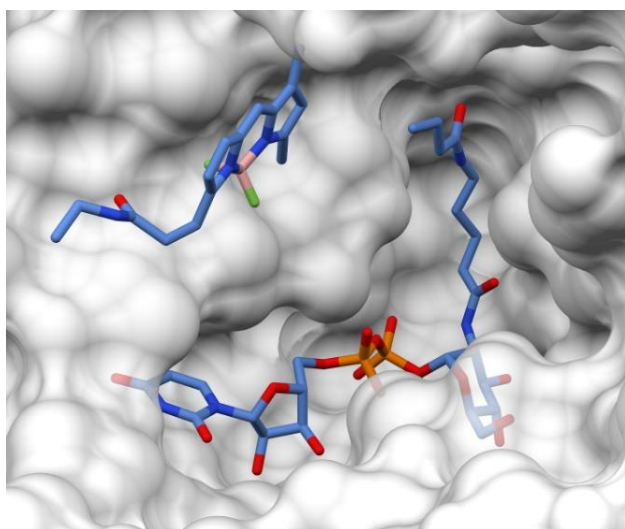


**Figure 2:** Crystallographic structure of OGT with substrate **2** bound. The OGT active site (grey) is depicted as a surface representation demonstrating how it is able to accommodate the caproic acid linker of the substrate (light blue). The fluorophore portion of a second substrate molecule can be modeled nearby.

Encouraged by these results, we set out to implement a convenient microplate-based assay (Figure 3). We envisioned we could incubate a biotinylated peptide as an OGT acceptor substrate along with glycosyl donor **2** and initiate the reaction through the addition of recombinant OGT to generate a BODIPY-modified glycopeptide. The modified and unmodified peptides can then be captured on streptavidin-coated surfaces after specified times. In this way, we reasoned we could directly monitor the glycosyl transfer catalyzed by OGT. We set out to use the same CKII peptide as noted above, which is a well-studied substrate of OGT and is readily prepared by solid-phase peptide synthesis, in its biotinylated form (Table S3) as a convenient acceptor substrate for the assay. The *N*-terminal biotin handle permitted immobilization on streptavidin-coated surfaces, which in turn facilitated subsequent washing to remove unreacted UDP-GlcN-BODIPY. The fluorescent signal remaining after washing could thus correspond to the BODIPY-modified glycopeptide, which can be obtained using a standard microplate reader (Figure S4). In this way, a measure of direct glycosyl transfer to a peptide acceptor can be obtained and a wide range of parameters can be varied to optimize the sensitivity of the assay. We found that both commercial streptavidin-coated microplates and streptavidin-coated magnetic beads could be used as a capture medium for the assay. We decided to use magnetic beads for subsequent experiments, since this format provided greater signal over background.

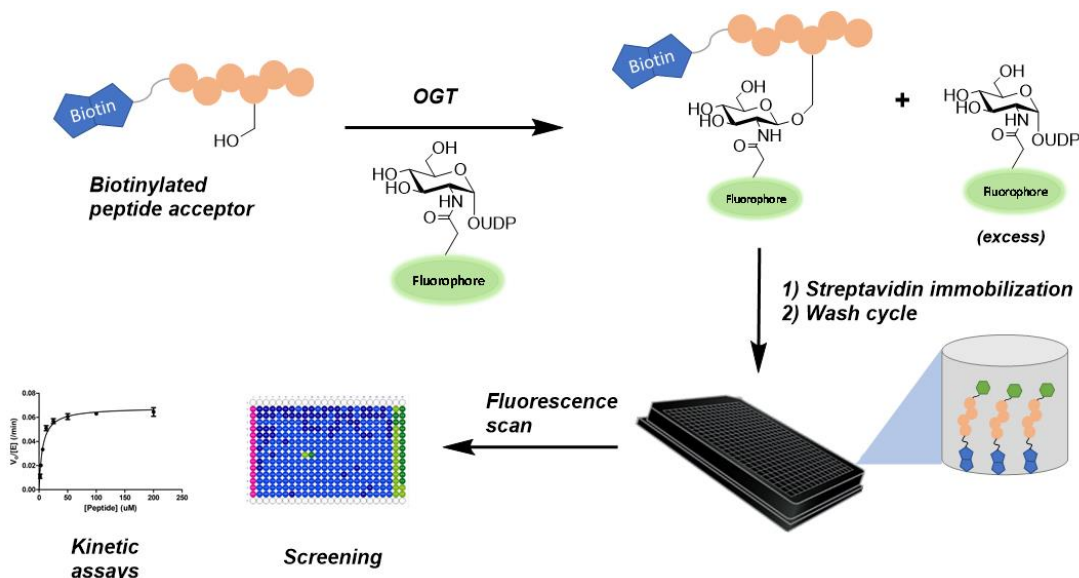


**Figure 3:** Methodology for activity-based OGT assay and inhibitor screen. Incubation of a peptide substrate with OGT results in transfer of a fluorescent sugar analogue. Immobilization on streptavidin-coated beads followed by washing permits direct measurement of transfer by fluorescence in 96- or 384-well plate format.

We recognized that one key factor in assay reproducibility would be to stop the assay at a defined time point by preventing further *O*-GlcNAc incorporation during the biotin-streptavidin capture. We reasoned that UDP, which is known to competitively inhibit OGT ( $K_i$  of  $1.3 \mu\text{M}$ )<sup>[40]</sup>, could be used to stop the enzymatic reaction prior to washing. Using this assay, we found that 2 mM UDP completely inhibits the reaction when concentrations of UDP-GlcN-BODIPY in the assay were equal or less than  $25 \mu\text{M}$  (Figure S5). After optimizing the assay conditions and concentrations of both substrates and OGT, we found that the assay produced fluorescence signals 50-fold greater than control reactions performed either in the presence of 2 mM UDP or in the absence of CKII peptide acceptor. By monitoring the reaction as a function of time at various concentrations of **2**, we were able to perform Michaelis-Menten analyses to obtain kinetic parameters for both the UDP-GlcN-BODIPY donor and CKII peptide acceptor (Figures 4A and 4B). As expected, the presence of the BODIPY fluorophore and linker impaired the rate of the reaction. This effect was quite modest, however, since the  $k_{\text{cat}}/K_M$  value for UDP-GlcN-BODIPY when using CKII as the acceptor was found to be  $\sim 7$ -fold lower than the value previously reported for  $\{^3\text{H}\}$ -UDP-GlcNAc when using a similar CKII peptide acceptor in a radioactivity-based assay (Table S2)<sup>[39]</sup>. Interestingly, the  $K_M^{\text{app}}$  for UDP-GlcN-BODIPY ( $K_M = 2.9 \pm 0.3 \mu\text{M}$ ) was found to be similar to that reported for UDP-GlcNAc ( $K_M = 2.3 \pm 0.4 \mu\text{M}$ ) and the reduction in  $k_{\text{cat}}$  value was approximately 6-fold ( $0.05 \pm 0.002 \text{ min}^{-1}$ ) as compared to the value measured for UDP-GlcNAc ( $0.29 \pm 0.01 \text{ min}^{-1}$ ) (Table S2). The similar  $K_M^{\text{app}}$  values observed for UDP-GlcNAc and UDP-GlcN-BODIPY, coupled with the structural data, suggest that OGT tolerates binding of the fluorophore and linker in its active site, and that the reduction in second order rate constant is largely driven by other factors affecting catalytic transfer to the peptide. We note that in the binary complex we observe the linker of compound **2**, and by extension the unmodeled fluorophore, reaches across the active site cleft to where the incoming peptide acceptor has been observed in ternary complexes<sup>[39]</sup>. We therefore reason that the linker or fluorophore may partially hinder binding of peptide acceptors, which may in turn explain the reduction in  $k_{\text{cat}}$  values observed using UDP-GlcN-BODIPY.

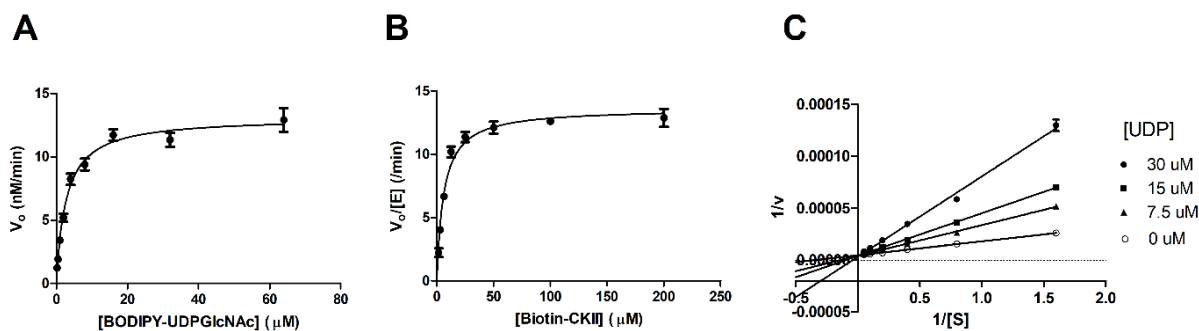


**Figure 4:** UDP-GlcN-BODIPY (**2**) is a substrate for OGT, permitting convenient determination of kinetic parameters. *A*, Michaelis-Menten curve of glycosyl donor **2** at saturating concentrations of peptide acceptor (>10-fold above  $K_M$ ). *B*, Michaelis-Menten curve of Biotin-CKII peptide acceptor in the presence of saturating concentrations of glycosyl donor. *C*, Lineweaver-Burk plot showing inhibition of OGT by UDP at varying concentrations of glycosyl donor **2**, with a calculated  $K_i$  value of 6.1  $\mu$ M. Error bars represent S.E.M. of triplicate measurements.

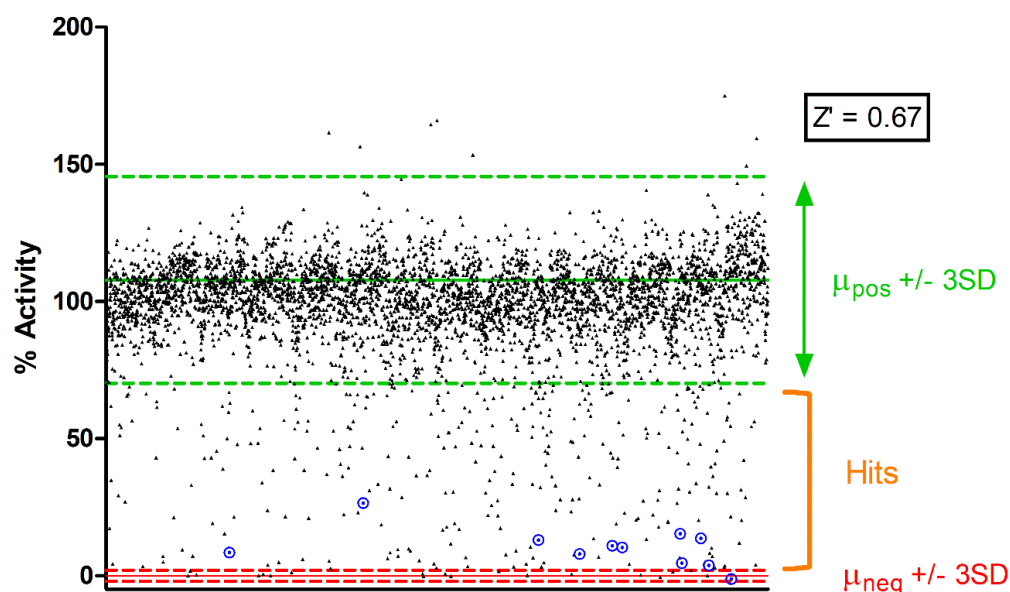
Next, having established initial conditions, we evaluated a small panel of biotinylated peptide acceptors that had been previously identified as OGT substrates (Figure S6). A TAK1-binding protein 1 (TAB-1) peptide<sup>[41]</sup> was found to have comparable kinetic parameters to those measured for CKII, whereas a peptide derived from host cell factor 1 (HCF-1)<sup>[42]</sup> was a 22-fold better substrate as determined by comparing its  $k_{cat}/K_M$  value to that obtained for CKII (Table S3). We therefore chose this peptide for subsequent studies since it produced greater signal to noise, even at lower concentrations of enzyme. We next investigated the utility of this assay for analysis of inhibitors, both in performing  $IC_{50}$  studies as well as for determining mode-of-inhibition and  $K_i$  values (Figure 4C). The inhibition of OGT using UDP and various concentrations of UDP-GlcN-BODIPY in the presence of saturating concentrations of the CKII peptide acceptor gave a  $K_i$  value of  $6.9 \pm 0.7 \mu$ M, which is in close agreement with previous reports using the radioactivity-based glycosyl transfer assay<sup>[43]</sup>. Lineweaver-Burk graphical analysis of this data also clearly showed the expected pattern of competitive inhibition. In contrast, when inhibition was assessed over varying concentrations of peptide acceptor, a non-competitive pattern of inhibition was obtained with respect to UDP (Figure S7). Importantly, these comparisons demonstrated the utility of our assay for the convenient determination of Michaelis-Menten parameters across various substrates and conditions as well as in detailed inhibition studies to establish the site at which an inhibitor binds within the active site of OGT.

Having demonstrated the applicability and high sensitivity of our assay in kinetic experiments, we next adapted the assay for use in 384-well microplates to enable economic use

of materials as well as with a view to apply it to high-throughput screening for small-molecule inhibitors of OGT. The concentration of donor and acceptor substrates used were at approximately  $K_M$  for each substrate in order to make the assay sensitive to compounds that might compete for binding at either the donor or acceptor binding site. The reaction buffer was also changed to include 0.01% (v/v) Triton X-100 so as to reduce potential non-specific inhibition by compounds prone to colloidal aggregation, which is a common problem encountered when performing screening assays<sup>[19]</sup>, and we reduced the total reaction volume to 25  $\mu$ L. These changes had no significant effect on assay behaviour. We also optimized the automated plate washing protocol to minimize disruption of the streptavidin-coated magnetic beads in the wells by introducing a short delay between wash cycles, which allows the beads to settle. We also adjusted the height at which aspiration was performed above the well base and found that a 6 mm height struck a balance between effective washing of the beads without aspirating them out of the wells, resulting in satisfactory signal-to-noise (Figure S8). Although we recognized that interference in screening could arise from antagonists that disrupt the biotin-streptavidin interaction, felt this extremely high affinity interaction would be one of the most robust binding interactions since the resulting complex has a half-life in the order of hours<sup>[44]</sup>. Accordingly, we reasoned that a 30 minute incubation time for capture would be sufficient to avoid interference. To test this assumption, we showed that desthiobiotin, a biotin analogue with a  $K_D$  of approximately  $10^{-11}$  M towards streptavidin<sup>[45]</sup>, at concentrations of up to 25  $\mu$ M did not influence the performance of the assay (Figure S9). This result suggested that the capture of the biotinylated substrate would not be impaired by even potent streptavidin antagonists, including less potent candidate antagonists that might be encountered during HTS.

Using this optimized assay, we next set out to validate this assay in high-throughput format by performing a trial screen. As a proof of concept, we used a targeted library containing 4480 known bioactive compounds obtained commercially from TargetMol Corp (Wellesley Hills, MA). We were able to conduct this assay over the course of one day in a fully automated format, which validated the suitability of this assay for high-throughput screening. The overall Z' score obtained for the assay was 0.67 (Figure 5) and we observed a clear Gaussian distribution of compound activities. Because the discovery of glycosyltransferase inhibitors from screening libraries has proved difficult, and identifying tractable inhibitors from past efforts to screen OGT has been challenging, we chose to screen using a relatively high compound concentration of 100  $\mu$ M. This translated to an overall hit rate of 6.1%, with hits being defined as those compounds resulting in OGT activity that was less than three standard deviations from the mean of our 100% activity control, which corresponds to 58.5% enzyme activity relative to the positive control vehicle only

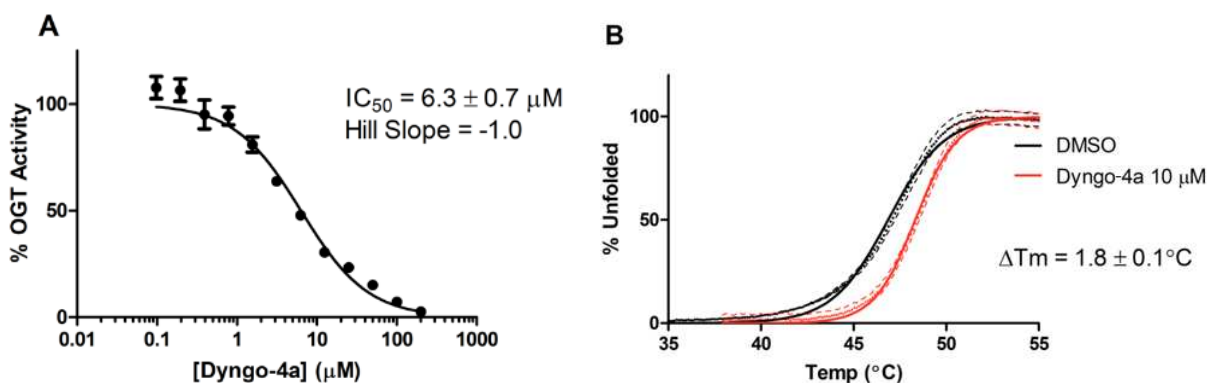
standards. Of the initial 275 hits we identified from primary screening, a short-list of 88 compounds for re-testing in triplicate was prepared by first excluding compounds in the library with a high likelihood of pan-assay interference (PAINS)<sup>[46]</sup> such as those that might function as detergents, or have fluorescent moieties or reactive functional groups. From these confirmed hits, we further prioritized 11 compounds that displayed desirable properties and obtained them commercially to determine inhibition constants. Compounds were also subjected to a secondary thermal shift assay using differential scanning fluorimetry (DSF)<sup>[47]</sup> to confirm direct binding of the materials to the enzyme.



**Figure 5:** Summary of screening results against OGT from a targeted library of 4480 known chemical probes. Compounds were screened at a final concentration of 100  $\mu\text{M}$ .  $\mu_{\text{pos}}$  corresponds to the mean signal of uninhibited positive control wells.  $\mu_{\text{neg}}$  corresponds to the mean signal of negative control wells in the absence of enzyme. Hits were defined as compounds resulting in less than 58.5% OGT activity, corresponding to at least three standard deviations from the positive control signal for activity. Prioritized hits which were selected for follow-up studies are marked as blue circles. Structures of these compounds and bioassay results are listed in the Supporting Information (Table S4).

Using our secondary binding assay in combination with our activity assay, we rejected the majority of our selected 11 hit compounds due to non-specific behaviour such as detergent sensitivity, solubility issues, or failure to replicate activity in both assay formats. However, we identified one compound (Dyngo<sup>®</sup>-4a, **9**, Table 1) which displayed low-micromolar affinity towards OGT in both our primary enzyme assay and secondary DSF assay. This compound was initially developed as part of a chemical family of inhibitors targeting the dynamin GTPase, an enzyme

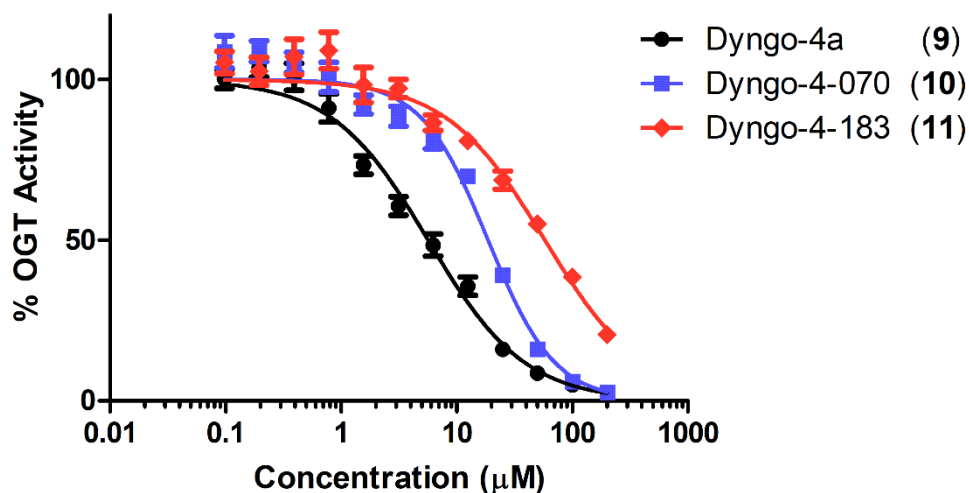
responsible for the rate-limiting scission of vesicles at the plasma membrane that occurs in many forms of endocytosis just prior to vesicle internalization<sup>[48,49]</sup>. Notably, Dyngo-4a represents a great improvement over its predecessor, known as Dynasore, both in terms of its potency against dynamin and consequent effects on endocytosis. Furthermore, Dyngo-4a exhibits desirable chemical properties including a lack of detergent sensitivity<sup>[49,50]</sup>. Given its utility in the inhibition of endocytosis, Dyngo-4a and other dynamin inhibitors have demonstrated efficacy in multiple proof-of-concept disease studies<sup>[51,52]</sup>. We were surprised to find that Dyngo-4a, which is a comparatively small molecule, also bound and inhibited OGT with an  $IC_{50}$  value of  $6.3 \pm 0.7 \mu\text{M}$  (Figure 6A). Using detailed kinetic assays, we showed that Dyngo-4a inhibits OGT non-competitively with respect to both the glycosyl donor and the peptide acceptor (Figure S10). Given the phenolic nature of Dyngo-4a, we speculated that it could lead to time dependent inactivation of OGT, but our kinetic studies show no time-dependent loss of activity, suggesting inhibition of OGT by Dyngo-4a is reversible (Figure S11). Additionally, the presence of 1 mM DTT in the assay buffer reduces the likelihood of oxidation of the phenolic hydroxyls to a quinone moiety. Furthermore, the positive shift in melting temperature observed when OGT is incubated with Dyngo-4a at a concentration of  $10 \mu\text{M}$ , coupled with the lack of detergent sensitivity and the Hill slope of -1, indicates that the compound directly binds and stabilizes the protein, rather than inactivating the enzyme non-specifically (Figure 6A and 6B).



**Figure 6:** Dyngo-4a binds and inhibits OGT with low-micromolar affinity. **A**, Concentration-response showing Dyngo-4a inhibition of recombinant OGT. Error bars represent S.E.M. ( $n=4$ ). **B**, DSF-based thermal shift assay showing thermal stabilization of the OGT catalytic domain in the presence of  $10 \mu\text{M}$  Dyngo-4a. Dashed lines indicate S.E.M ( $n=3$ ). A temperature ramp of  $25^{\circ}\text{C}$  to  $95^{\circ}\text{C}$  was used at a gradient of  $0.05^{\circ}\text{C}/\text{sec}$ .

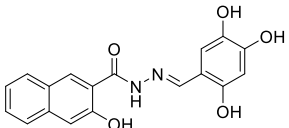
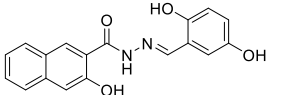
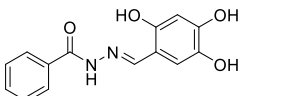
Although we were encouraged by the ability of Dyngo-4a to inhibit OGT, we recognized that this off-target inhibition would complicate future studies of this tool compound, both for potential use

as an OGT inhibitor but also for use as a dynamin inhibitor. We therefore aimed to identify structurally related compounds that would inhibit each target in a selective manner by testing previously-synthesized Dyngo-4a analogues against OGT. Through screening of a small library of 167 Dyngo-4a analogues, we identified an additional 9 compounds that showed at least 50% inhibition against OGT at a concentration of 40  $\mu\text{M}$  (Figure S12). Two of these compounds display minimal activity towards dynamin, but largely retain their potency toward OGT (Figure 7). Compound **10**, which differs from the parent compound by the removal of one hydroxyl group, retains an  $\text{IC}_{50}$  value for OGT of  $19 \pm 3 \mu\text{M}$  (Table 1). Compound **11** displays less potency towards OGT but also displays selectivity, as no inhibition towards dynamin was observed at concentrations up to 100  $\mu\text{M}$  (Table 1, Figure S13). These compounds should serve as a small novel scaffold from which more potent analogues can be derived. Additionally, the results obtained here highlight the utility of our assay for the quick identification of Dyngo-4a analogues that do not show inhibition towards OGT, suggesting that the development of more potent and selective effectors of dynamin activity is also feasible.



**Figure 7:** Screening of a series of Dyngo-4a analogues reveals two additional compounds with selectivity for OGT. Concentration response curves show inhibition of recombinant OGT by Dyngo-4a (**9**, black), and structurally related analogues **10** (blue), and **11** (red). Error bars represent S.E.M. of triplicate measurements.



Compound	Structure	IC <sub>50</sub> (OGT)	IC <sub>50</sub> (DynI)
Dyngo-4a (9)		6.3 ± 0.7 μM	2.7 ± 0.7 μM
Dyngo-4-070 (10)		19 ± 2 μM	33 ± 0.7 μM
Dyngo-4-183 (11)		58 ± 9 μM	> 100 μM

**Table 1:** Comparison of biological activity observed from Dyngo-4a (9) and related analogues (10,11).

## Conclusions

Owing to the important roles played by glycosyltransferases, the development of inhibitors of these enzymes is currently a topic of high interest. A prerequisite for successful identification of such inhibitors is the development of robust assays for this class of enzymes. Remarkably few GT assays are known in which the assay reports directly on the enzyme catalyzed transfer of the carbohydrate unit. Here we exploit the substrate tolerance of OGT to develop what is, to our knowledge, the first fluorescence-based assay that reports directly on the transfer of the sugar unit. Optimization of this assay yields a highly sensitive and accurate assay that can be conveniently used to obtain Michaelis-Menten kinetic parameters for both substrates and inhibitors. This assay is furthermore amenable for use in high-throughput screening. After HTS-based discovery of a known endocytosis inhibitor in a screening campaign, we used this assay to rapidly assess a family of analogues in order to identify a selective OGT inhibitor. While these leads show relatively modest potency, the low molecular weight of these compounds may make them a useful starting point to generate tool compounds for OGT and provide a novel scaffold for development of more potent analogues. We expect this assay will have great utility, both for routine kinetic analysis of OGT activity as well as for additional HTS campaigns for inhibitors of OGT.

While the substrates used in this assay are tailored for OGT, we note that many glycosyltransferases that have been studied in this regard demonstrate tolerance for pendant groups<sup>[4,15,17,53]</sup>. Although the degree of tolerance is highly dependent on the individual enzyme, it

is likely that similar fluorescent substrates can be developed for other GTs but may require optimization of both the type of linker and its site of attachment. Therefore, we believe this assay format could be readily adapted to other families of GTs, including those that have already been shown to tolerate pendent groups including fucosyltransferases<sup>[4,54,55]</sup>, sialyltransferases<sup>[4,55]</sup>, and polypeptide GalNAc transferases<sup>[56]</sup>. Combining the use of such fluorescent donor sugars with biotinylated acceptors will permit the study of these other classes of GTs. An advantage of our assay is that it is compatible for use with GTs that use non-Leloir glycosyl donors, which cannot be monitored by coupled assays that detect nucleotide diphosphate reaction products. Additionally, as a screening assay, our approach is capable of robust and efficient HTS and can detect weak (>50  $\mu$ M) binders, which is useful for GTs as these are notoriously difficult to target. The ability to screen with low concentrations of enzyme (20 nM), as well as low donor (3  $\mu$ M) and acceptor substrates (10  $\mu$ M), makes this approach reagent conservative and therefore readily feasible for high throughput screening. Notably, this flexibility also permits the design of screens that are biased toward a particular type of inhibition – for example, by increasing the concentration of one substrate or the other above  $K_M$  in order to select for non-competitive or allosteric inhibitors. We also note that the strategy of directly incorporating the fluorescent reporter to a substrate, adding magnetic beads to the reaction wells, and then measuring on-bead fluorescence after washing offers a simplified assay design that minimizes reagent transfer and liquid handling steps. We therefore expect this general assay format will aid in the mission of discovering improved chemical tools for the important superfamily of glycosyltransferases. Finally, we believe that this technique will have applications for other group transfer enzymes that are difficult to monitor directly including, for example, acyltransferases and nucleic acid polymerases.

### ***Acknowledgements***

D.J.V. is supported by a Tier I Canada Research Chair in Chemical Glycobiology and an E.W.R. Steacie Memorial Fellowship. Additional financial support was provided by the Canadian Glycomics Network (R675184) and a Discovery Grant from the Natural Sciences and Engineering Research Council (RGPIN-2015-05426). The miniaturization of the assay and the high throughput screening campaign were performed in the Center for High Throughput Chemical Biology (HTCB) at Simon Fraser University. The HTCB is supported by grants from the Canadian Foundation for Innovation (Innovation Fund Grant Number 33097, JELF Grant Number 36766, and JELF Grant Number 37241), the British Columbia Knowledge Development Foundation (Grant Numbers 662-805223 and 862-805636), and the Y.P. Heung Foundation. We would like to thank Diamond Light

Source for access to beamline I04-1 (proposal number mx18598). GJD thanks the Royal Society for the Ken Murray Research Professorship and RWM for the associated PDRA funding (RP\EA\180016). P.J.R. and A.M are supported by the National Health & Medical Research Council Australia (GNT1162515 and GNT1137064), the Australian Research Council (DP180101781) and for equipment from the Australian Cancer Research Foundation, the Ramaciotti Foundation and the Cancer Institute NSW.

### **Competing Interests**

Dyngo<sup>®</sup> is a registered trademark of Newcastle Innovation Ltd and Children's Medical Research Institute and some of the Dyngo<sup>®</sup> compounds are commercially available to researchers via Abcam Biochemicals<sup>®</sup> (Cambridge, UK).

### **References:**

- [1] A. Varki, *Glycobiology* **2017**, *27*, 3–49.
- [2] L. L. Lairson, B. Henrissat, G. J. Davies, S. G. Withers, *Annu. Rev. Biochem.* **2008**, *77*, 521–555.
- [3] S. S. Pinho, C. A. Reis, *Nat. Rev. Cancer* **2015**, *15*, 540–555.
- [4] C. D. Rillahan, S. J. Brown, A. C. Register, H. Rosen, J. C. Paulson, *Angew. Chemie - Int. Ed.* **2011**, *50*, 12534–12537.
- [5] C. W. Hall, T. F. Mah, *FEMS Microbiol. Rev.* **2017**, *41*, 276–301.
- [6] J. Marshall, Y. Sun, D. S. Bangari, E. Budman, H. Park, J. B. Nietupski, A. Allaire, M. A. Cromwell, B. Wang, G. A. Grabowski, et al., *Mol. Ther.* **2016**, *24*, 1019–1029.
- [7] G. K. Wagner, T. Pesnot, *ChemBioChem* **2010**, *11*, 1939–1949.
- [8] Z. L. Wu, C. M. Ethen, B. Prather, M. Machacek, W. Jiang, *Glycobiology* **2011**, *21*, 727–733.
- [9] O. von Ahsen, U. Voigtmann, M. Klotz, N. Nifantiev, A. Schottelius, A. Ernst, B. Müller-Tiemann, K. Parczyk, *Anal. Biochem.* **2008**, *372*, 96–105.
- [10] W. A. Lubas, J. A. Hanover, *J. Biol. Chem.* **2000**, *275*, 10983–10988.
- [11] J. J. M. Bergeron, R. A. Rachubinski, R. A. Sikstrom, B. I. Posner, J. Paiement, *J. Cell Biol.* **1982**, *92*, 139–146.
- [12] S. Gosselin, M. Alhussaini, M. H. Streiff, K. Takabayashi, M. M. Palcic, *Anal. Biochem.* **1994**, *220*, 92–97.

- [13] S. Zegzouti, H., Engel, L., Hennek, J., Alves, J., Vidugiris, G., Goueli, S., *Glycobiology* **2014**, *24*, 1051.
- [14] J. Qi, R. Wang, Y. Zeng, W. Yu, Y. Gu, *Prep. Biochem. Biotechnol.* **2017**, *47*, 699–702.
- [15] X. Zhang, F. Chen, A. Petrella, F. Chacón-Huete, J. Covone, T.-W. Tsai, C.-C. Yu, P. Forgione, D. H. Kwan, *ACS Chem. Biol.* **2019**, *14*, 715–724.
- [16] B. J. Gross, B. C. Kraybill, S. Walker, *J. Am. Chem. Soc.* **2005**, *127*, 14588–14589.
- [17] Z. Gao, O. G. Ovchinnikova, B.-S. Huang, F. Liu, D. E. Williams, R. J. Andersen, T. L. Lowary, C. Whitfield, S. G. Withers, **2019**, DOI 10.1021/jacs.8b10940.
- [18] M. G. Acker, D. S. Auld, *Perspect. Sci.* **2014**, *1*, 56–73.
- [19] B. Y. Feng, A. Simeonov, A. Jadhav, K. Babaoglu, J. Inglese, B. K. Shoichet, C. P. Austin, *J. Med. Chem.* **2007**, *50*, 2385–2390.
- [20] W. A. Lea, A. Simeonov, *Expert Opin. Drug Discov.* **2011**, *6*, 17–32.
- [21] A. Wochner, J. Glökler, *Biotechniques* **2007**, *42*, 578–582.
- [22] T. Carmen-Rosa, G. W. Hart, *J. Biol. Chem.* **1984**, *259*, 3308–3317.
- [23] X. Yang, K. Qian, *Nat. Rev. Mol. Cell Biol.* **2017**, *18*, 452–465.
- [24] J. C. Trinidad, D. T. Barkan, B. F. Gullledge, A. Thalhammer, A. Sali, R. Schoepfer, A. L. Burlingame, *Mol. Cell. Proteomics* **2012**, *11*, 215–229.
- [25] S. Brimble, E. Wollaston-Hayden, C. Teo, A. Morris, L. Wells, *Curr. Signal Transduct. Ther.* **2010**, *5*, 12–24.
- [26] J. A. Groves, A. Lee, G. Yildirim, N. E. Zachara, *Cell Stress Chaperones* **2013**, *18*, 535–558.
- [27] F. Capotosti, S. Guernier, F. Lammers, P. Waridel, Y. Cai, J. Jin, J. W. Conaway, R. C. Conaway, W. Herr, *Cell* **2011**, *144*, 376–388.
- [28] J. A. Hanover, W. Chen, M. R. Bond, *J. Bioenerg. Biomembr.* **2018**, *50*, 155–173.
- [29] C. M. Ferrer, T. Y. Lu, Z. A. Bacigalupa, C. D. Katsetos, D. A. Sinclair, M. J. Reginato, *Oncogene* **2017**, *36*, 559–569.
- [30] T. P. Lynch, C. M. Ferrer, S. R. E. Jackson, K. S. Shahriari, K. Vosseller, M. J. Reginato, *J. Biol. Chem.* **2012**, *287*, 11070–11081.
- [31] R. M. De Queiroz, R. Madan, J. Chien, W. B. Dias, C. Slawson, *J. Biol. Chem.* **2016**, *291*, 18897–18914.
- [32] B. J. Gross, J. G. Swoboda, S. Walker, *J. Am. Chem. Soc.* **2008**, *130*, 440–441.
- [33] R. F. Ortiz-Meoz, J. Jiang, M. B. Lazarus, M. Orman, J. Janetzko, C. Fan, D. Y. Duveau, Z. W. Tan, C. J. Thomas, S. Walker, *ACS Chem. Biol.* **2015**, *10*, 1392–1397.
- [34] S. E. S. Martin, Z. W. Tan, H. M. Itkonen, D. Y. Duveau, J. A. Paulo, J. Janetzko, P. L. Boutz, L. Törk, F. A. Moss, C. J. Thomas, et al., *J. Am. Chem. Soc.* **2018**, *140*, 13542–13545.
- [35] R. Trapannone, K. Rafie, D. M. F. Van Aalten, *Biochem. Soc. Trans.* **2016**, *44*, DOI

10.1042/BST20150189.

- [36] E. J. Kim, L. K. Abramowitz, M. R. Bond, D. C. Love, D. W. Kang, H. F. Leucke, D. W. Kang, J. S. Ahn, J. A. Hanover, *Bioconjug. Chem.* **2014**, *25*, 1025–1030.
- [37] H. Y. Tan, R. Eskandari, D. Shen, Y. Zhu, T. W. Liu, L. I. Willems, M. G. Alteen, Z. Madden, D. J. Vocadlo, *J. Am. Chem. Soc.* **2018**, *140*, 15300–15308.
- [38] D. L. MacDonald, *J. Org. Chem.* **1962**, *27*, 1107–1109.
- [39] M. B. Lazarus, Y. Nam, J. Jiang, P. Sliz, S. Walker, *Nature* **2011**, *469*, 564–569.
- [40] K. Rafie, A. Gorelik, R. Trapannone, V. S. Borodkin, D. M. F. van Aalten, *Bioconjug. Chem.* **2018**, *29*, 1834–1840.
- [41] S. Pathak, V. S. Borodkin, O. Albarbarawi, D. G. Campbell, A. Ibrahim, D. M. van Aalten, *EMBO J.* **2012**, *31*, 1394–1404.
- [42] M. B. Lazarus, J. Jiang, T. M. Gloster, W. F. Zandberg, G. E. Whitworth, D. J. Vocadlo, S. Walker, *Nat. Chem. Biol.* **2012**, *8*, 966–968.
- [43] D. L. Shen, T. M. Gloster, S. A. Yuzwa, D. J. Vocadlo, *J. Biol. Chem.* **2012**, *287*, 15395–15408.
- [44] A. Chilkoti, P. S. Stayton, *Molecular Origins of the Slow Streptavidin-Biotin Dissociation Kinetics*, **1995**.
- [45] J. D. Hirsch, L. Eslamizar, B. J. Filanoski, N. Malekzadeh, R. P. Haugland, J. M. Beechem, R. P. Haugland, *Anal. Biochem.* **2002**, *308*, 343–357.
- [46] J. B. Baell, J. W. M. Nissink, *ACS Chem. Biol.* **2018**, *13*, 36–44.
- [47] F. H. Niesen, H. Berglund, M. Vedadi, *Nat. Protoc.* **2007**, *2*, 2212–2221.
- [48] G. J. Doherty, H. T. McMahon, *Annu. Rev. Biochem.* **2009**, *78*, 857–902.
- [49] A. McCluskey, J. A. Daniel, G. Hadzic, N. Chau, E. L. Clayton, A. Mariana, A. Whiting, N. N. Gorgani, J. Lloyd, A. Quan, et al., *Traffic* **2013**, *14*, 1272–1289.
- [50] E. Macia, M. Ehrlich, R. Massol, E. Boucrot, C. Brunner, T. Kirchhausen, *Dev. Cell* **2006**, *10*, 839–850.
- [51] C. B. Harper, S. Martin, T. H. Nguyen, S. J. Daniels, N. A. Lavidis, M. R. Popoff, G. Hadzic, A. Mariana, N. Chau, A. McCluskey, et al., *J. Biol. Chem.* **2011**, *286*, 35966–35976.
- [52] Y. Y. Li, X. N. Chen, X. X. Fan, Y. J. Zhang, J. Gu, X. W. Fu, Z. H. Wang, X. F. Wang, Z. Xiao, *Synapse* **2015**, *69*, 67–77.
- [53] M. Noel, P. A. Gilormini, V. Cogez, N. Yamakawa, D. Vicogne, C. Lion, C. Biot, Y. Guérardel, A. Harduin-Lepers, *ChemBioChem* **2017**, *18*, 1251–1259.
- [54] T. Maeda, S.-I. Nishimura, *Chem. - A Eur. J.* **2008**, *14*, 478–487.
- [55] S. Hong, P. Sahai-Hernandez, D. G. Chapla, K. W. Moremen, D. Traver, P. Wu, *Angew. Chemie Int. Ed.* **2019**, *58*, 14327–14333.
- [56] H. C. Hang, C. Yu, M. R. Pratt, C. R. Bertozzi, *J. Am. Chem. Soc.* **2004**, *126*, 6–7.



## SUPPLEMENTAL FIGURES

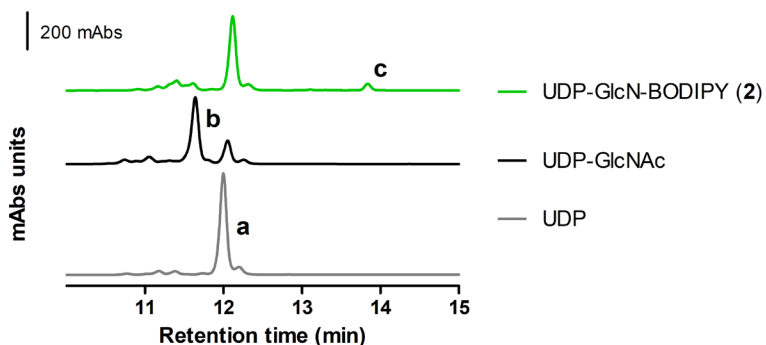


**Figure S1: UDP-GlcN-BODIPY (2) is a substrate for OGT** Glycosylation of a TAMRA-labeled CKII peptide acceptor using either UDP (grey), UDP-GlcNAc (blue) or UDP-GlcN-BODIPY (green) was monitored by LC/MS after 3 hours incubation at 37°C. **a**, CKII (RT = 12.1 min,  $m/z = 906.2 [M+2H]^{2+}$ ), **b**, CKII-GlcNAc (RT = 11.5 min,  $m/z = 1007.5 [M+2H]^{2+}$ ), **c** CKII- GlcN-BODIPY (RT = 13.7 min,  $m/z = 1130.5[M+2H]^{2+}$ ). Reaction mixtures consisted of 100  $\mu\text{M}$  nucleotide sugar donor, 100  $\mu\text{M}$  CKII peptide, 1  $\mu\text{M}$  recombinant OGT, and 5U alkaline phosphatase in PBS containing 12.5 mM  $\text{MgCl}_2$ . LC/MS was performed according to the method described in General Procedures (mobile phase  $\text{H}_2\text{O}/\text{CH}_3\text{CN} + 0.1\%$  TFA, 30 to 70%  $\text{CH}_3\text{CN}$  over 20 min).

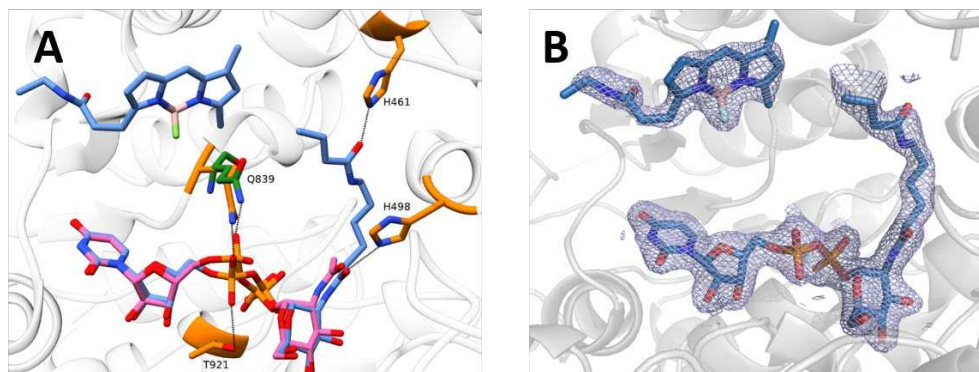


**Figure S2: The OGT active site accommodates substrate 2 with minimal disruption.** **A**, Structure of UDP-GlcNAc bound OGT (PDB= 4gz5, pink for UDP-GlcNAc, green for OGT residues) overlaid onto OGT/substrate 2 complex, indicating substrates are similarly positioned except for the  $\alpha$ -phosphate. OGT structure depicted as translucent cartoon ribbons with residues discussed in main body of text shown in orange and substrate 2 in light blue. Hydrogen bonds depicted as black lines. **B**, Final  $2F_o - F_c$  electron density map for substrate 2. Electron density contoured to  $1\sigma$  and depicted as a blue mesh around ligands (light blue sticks).

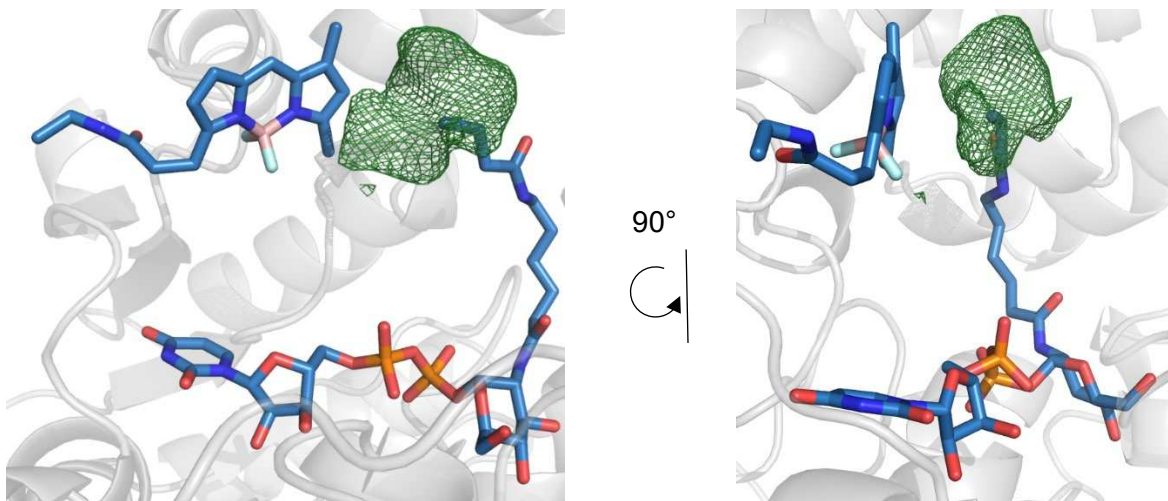


**Figure S3: The omit  $F_o-F_c$  electron density map for the unmodeled BODIPY fluorophore.** Difference density contoured to  $3\sigma$  and depicted as green mesh above the 5-carbon linker of substrate **2**. Difference density could not be modelled with confidence, likely attributable to multiple BODIPY conformations.

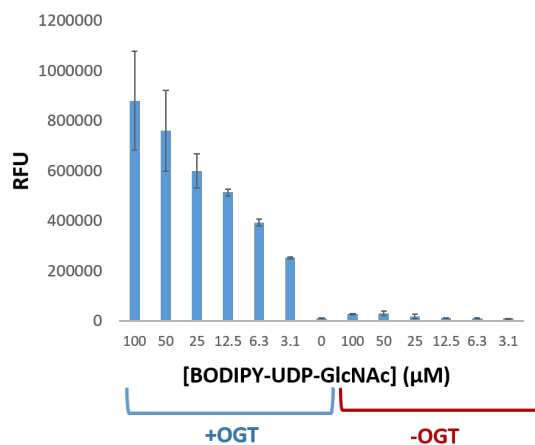


**Figure S4: BODIPY-UDP-GlcNAc (**2**) is processed by OGT in a concentration-dependent manner and produces >50-fold signal/background.** 100 μM Biotin-CKII peptide was incubated with 200 nM OGT in PBS at 37°C for 3 hours. Samples were then transferred to streptavidin-coated microplates, washed 5 times with PBS, and read at 490/525 Ex/Em fluorescence. Error bars represent S.E.M. of triplicate samples.



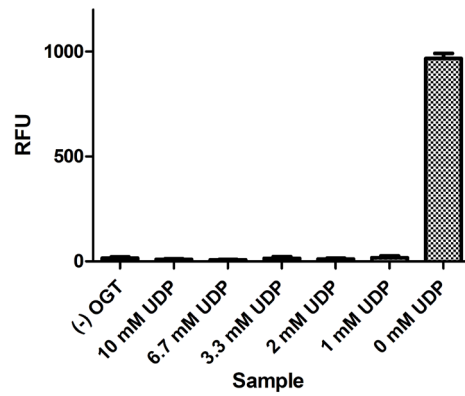


**Figure S5: UDP concentrations  $\geq 1$  mM are sufficient to inhibit 99% of OGT activity, making it suitable as a stop reagent for the activity assay.** Assay was performed according to the general procedure (Supplemental Methods) using 3  $\mu$ M substrate **2**, 12.5  $\mu$ M Biotin-CKII peptide, and 250 nM OGT. Reaction components were combined with various concentrations of UDP and incubated at room temperature for 3 hours. Error bars represent S.E.M. of triplicate values.

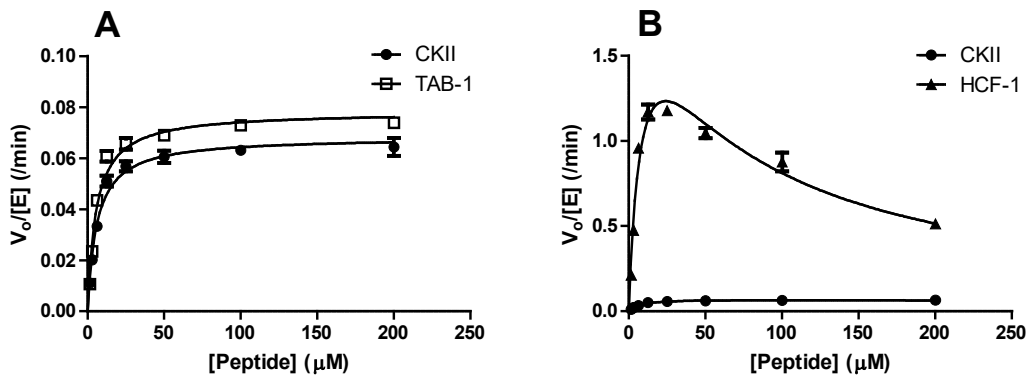


**Figure S6: Fluorescent assay permits comparison of OGT-catalyzed glycosylation of various peptide acceptors.** A, Michaelis-Menten plot detailing glycosylation kinetics of CKII vs TAB-1. OGT displays typical Michaelis-Menten behaviour in the presence of these substrates, with similar second-order rate constants (Table S3). Curves were fitted to a standard Michaelis-Menten equation using Graphpad Prism. B, Michaelis-Menten plot detailing glycosylation of CKII vs HCF-1. Substrate or product inhibition was observed for HCF-1 irrespective of enzyme concentration. Reaction progress curves were found to be linear for the duration of the read at all concentrations tested. OGT displays a higher affinity for this substrate relative to CKII, with a 21-fold difference in second-order rate constants (Table S3). Data for HCF-1 was fitted to the equation incorporating substrate inhibition [ $Y = V_{max} * X / (K_m + X * (1 + X/K_i))$ ]. Error bars represent S.E.M. of quadruplicate measurements.

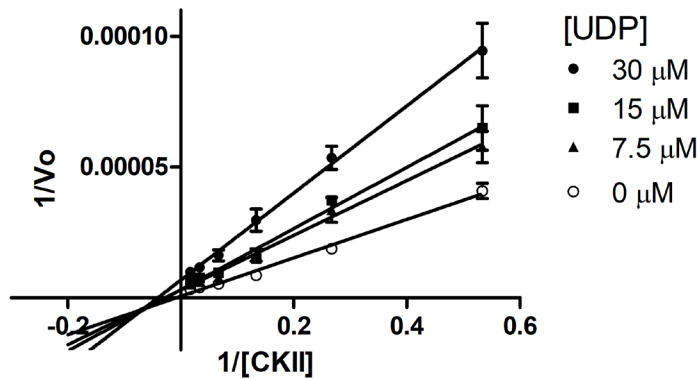


**Figure S7: UDP inhibits OGT non-competitively with respect to CKII acceptor peptide.** Initial rates of OGT-catalyzed glycosylation of CKII in the presence of varying concentrations of UDP and CKII, and a fixed concentration of UDP-GlcN-BODIPY (30  $\mu\text{M}$ ), were transformed into a double-reciprocal plot.  $K_i$  values were calculated from non-linear regression of Michaelis-Menten curves. Calculated UDP  $K_i = 15 \mu\text{M}$ . Error bars represent S.E.M. of triplicate measurements.

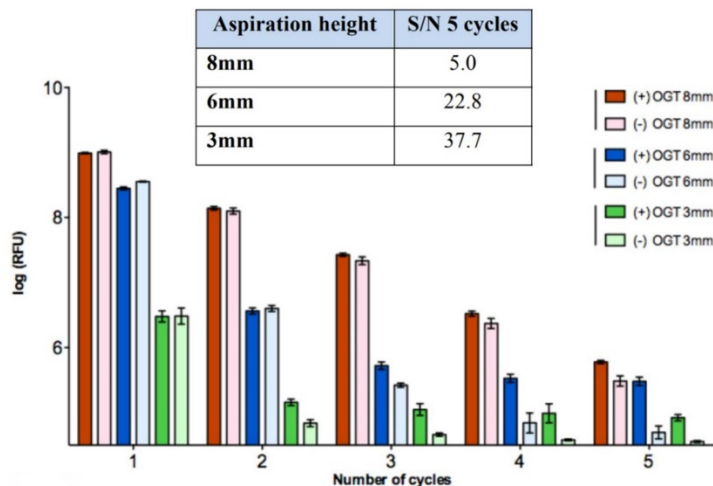


**Figure S8: Optimization of automated plate washer cycles indicates that a 6 mm aspiration height results in excellent signal-to-noise between controls.** A lower height setting (3 mm) results in loss of overall signal, suggesting that some beads containing glycosylated product are aspirated. 384-well plates were washed with 100  $\mu\text{L}$  PBS per cycle using a BioTek EL406 automated plate washer. A final dispense step of 50  $\mu\text{L}$  PBS was performed prior to reading the plates. Error bars represent S.E.M. of triplicate values.

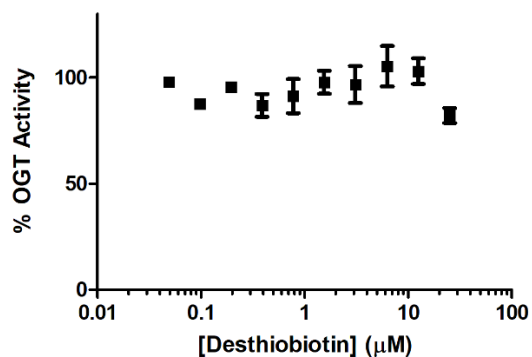


**Figure S9: The presence of desthiobiotin does not significantly affect assay performance at concentrations up to 25 μM.** The reported  $K_D$  for desthiobiotin is approximately  $10^{-11}$  M [1]. Assay was performed according to the general procedure using 3 μM substrate **2**, 10 μM Biotin-HCF-1 peptide, and 20 nM OGT. Reactions were carried out at room temperature for 60 min and were stopped by addition of UDP to a final concentration of 2 mM. Error bars represent S.E.M. of triplicate measurements.

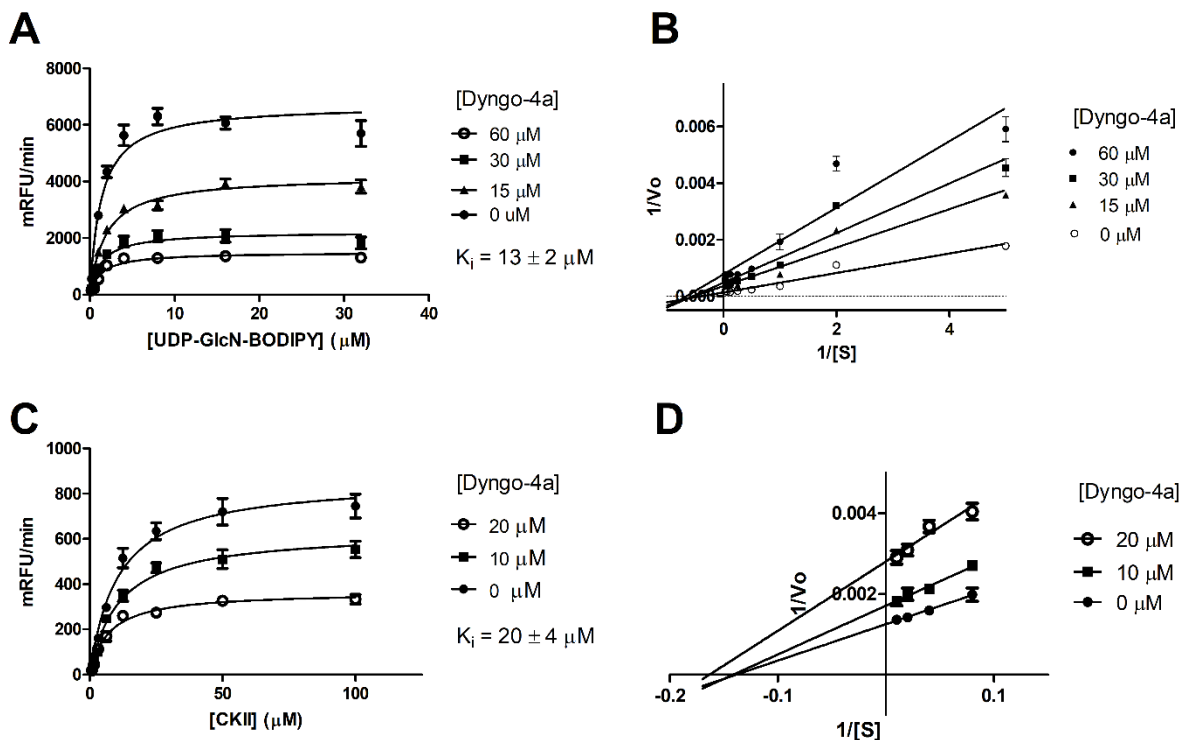


**Figure S10: Dyngo-4a inhibits OGT non-competitively with respect to both glycosyl donor and acceptor substrates.** *A*, Michaelis-Menten plots of UDP-GlcN-BODIPY (**2**) in the presence of varying concentrations of Dyngo-4a (**9**). Increasing concentrations of **9** result in a reduction of  $V_{\text{max}}$  without significantly affecting  $K_M$ . *B*, double-reciprocal plot of Michaelis-Menten data demonstrating a non-competitive pattern of inhibition. *C*, Michaelis-Menten plots of CKII peptide in the presence of varying concentrations of **9**, which reduces  $V_{\text{max}}$  but does not affect  $K_M$ . *D*, double-reciprocal plot of CKII Michaelis-Menten data, demonstrating a non-competitive pattern of inhibition.  $K_i$  values were calculated from non-linear regression of Michaelis-Menten curves using Graphpad Prism 5. Error bars represent S.E.M. of quadruplicate measurements.

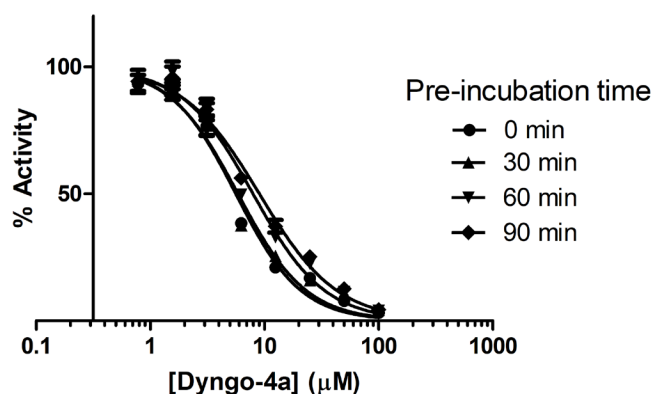


**Figure S11: Dyngo-4a does not inhibit OGT in a time-dependent fashion.** Enzyme was pre-incubated with OGT at 4°C for 0-90 minutes prior to addition of substrate and relative activity was normalized against controls containing no inhibitor or no enzyme. Calculated IC<sub>50</sub> values range from 5.6 to 9.0 μM.

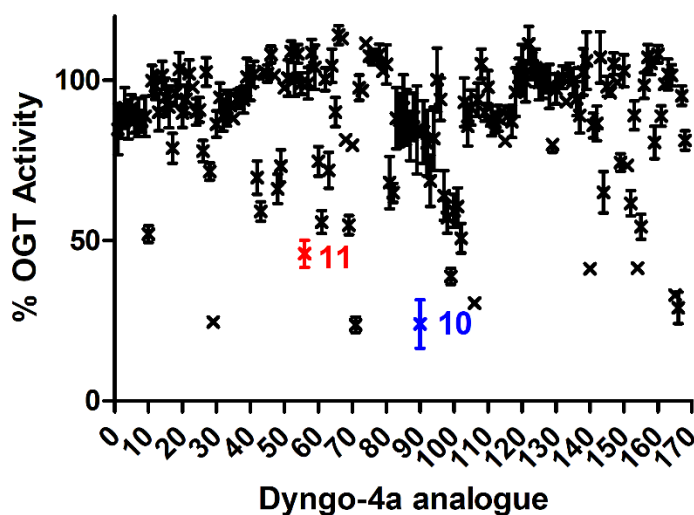


**Figure S12: Screening of 167 structurally-related analogues of Dyngo-4a reveals additional inhibitors of OGT.** Compounds were screened at a final concentration of 40 μM under balanced assay conditions identical to those used for high-throughput screening of OGT. Prioritized analogues Dyngo-4-070 (**10**) and Dyngo-4-183 (**11**) are indicated in blue and red font, respectively. Compounds were assayed in triplicate; error bars represent S.E.M.

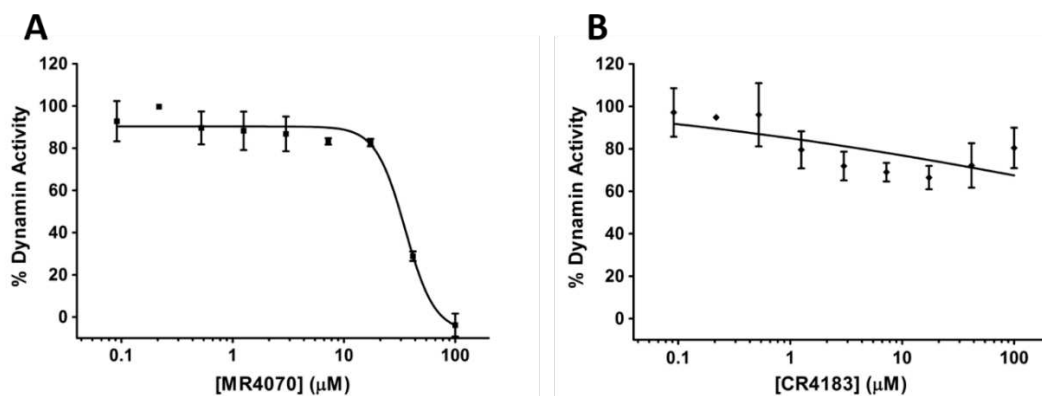


**Figure S13: Effect of Dyngo analogues on dynamin GTPase activity.** A, Dyngo-4-070 (10), B, Dyngo-4-183 (11). Assay was performed according to the general procedure for *in vitro* dynamin activity in three independent experiments, each with technical triplicates.

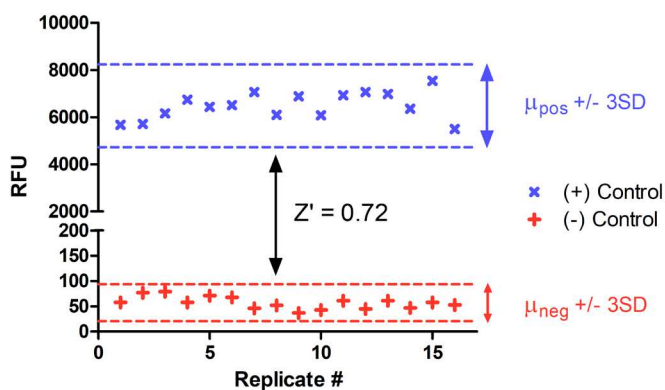


**Figure S14: Optimized conditions for fluorescent activity assay result in robust signal/noise and Z'-scores suitable for HTS.** A representative control plate was subjected to identical conditions described in the general HTS procedure. Z' score was calculated according to equation 1 described by Zhang *et al.*<sup>[2]</sup>:

$$Z' = 1 - \frac{3(\sigma_{c+} + \sigma_{c-})}{|\mu_{c+} - \mu_{c-}|} \quad (1)$$

Where  $\sigma$  is the standard deviation of the positive and negative control replicates and  $\mu$  is the mean of the control replicates. Positive controls consisted of reaction wells in the absence of inhibitor; negative controls consisted of reaction wells in the absence of enzyme.

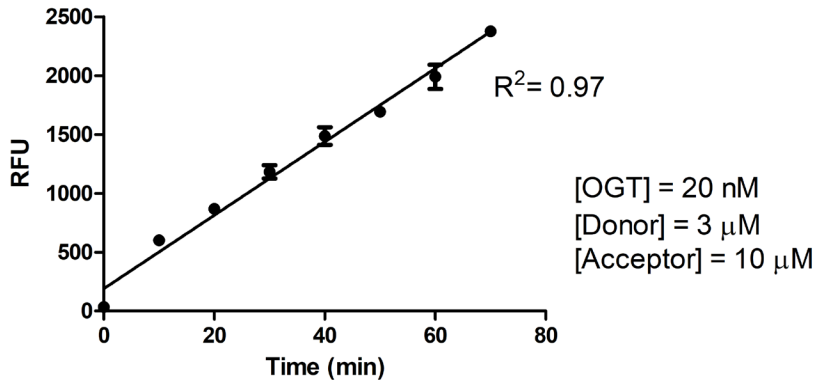


**Figure S15: Conditions used for high-throughput screening result in linear reaction progress curves for at least 75 minutes when using 20 nM OGT.** Experiments were performed according to the general procedure of the OGT activity assay using donor and acceptor substrate concentrations  $\approx K_M$  (3  $\mu\text{M}$  and 10  $\mu\text{M}$ , respectively). Wells at various time points were stopped by the addition of an equal volume of 7.5 mM UDP to the reaction. Data points represent S.E.M of four replicate measurements.

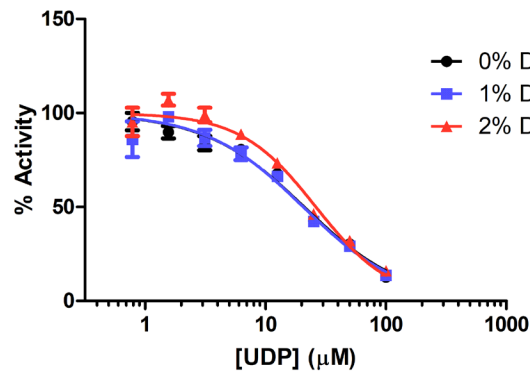


**Figure S16: Concentrations of up to 2% DMSO do not significantly affect the performance of the fluorescent OGT assay.** Assay was performed according to the general procedure using 3  $\mu\text{M}$  substrate 2, 12.5  $\mu\text{M}$  Biotin-CKII peptide, and 200 nM OGT. UDP was pre-incubated with enzyme at 4°C for 30 min prior to addition of substrates. Reactions were carried out at room temperature for 60 min and were stopped by addition of UDP to a final concentration of 2.5 mM. Data were fitted to normalized 4-parameter sigmoidal inhibition curve using Graphpad Prism 5. Error bars represent S.E.M. of triplicate values.

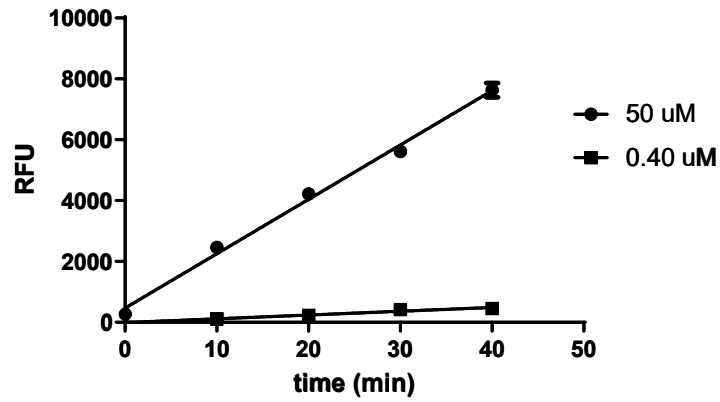


**Figure S17: Glycosylation kinetics of HCF-1 are linear over all concentrations of Substrate 2.** Final concentration of OGT is 20 nM. Assay was performed according to the general procedure using a fixed concentration of HCF-1 peptide (10  $\mu$ M,  $\approx K_M$ ). Reactions were stopped at various time points with the addition of 2 mM UDP. Error bars represent S.E.M. of quadruplicate measurements.



<b>OGT4.5 with substrate 2</b>	
Accession Code	6TKA
<b>Data Collection</b>	
Space Group	P3 <sub>1</sub> 21
Cell Dimensions	
a, b, c (Å)	100.8, 100.8, 132.6
α, β, γ (°)	90, 90, 120
Resolution (Å)	87.32 (1.91)*
R <sub>merge</sub>	0.096 (2.332)
R <sub>p.i.m</sub>	0.03 (0.710)
I/σI	15.6 (1.1)
CC <sub>1/2</sub>	1 (0.405)
Completeness (%)	100 (100)
Redundancy	12 (12.3)
<b>Refinement</b>	
Resolution (Å)	1.91-73.05
No. of reflections	57876
R <sub>work</sub> /R <sub>free</sub>	18.4/23.3
No. of atoms	
Protein	5609
Ligand	72
Water	208
<b>B-factors</b>	
Protein	41.65
Ligand/ion	46.06
Water	41.20
<b>R.m.s deviations</b>	
Bond lengths (Å)	0.009
Bond angles (°)	1.57

**Table S1: Data collection of refinement statistics for 6TKA**

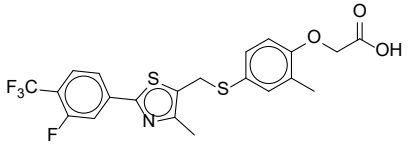
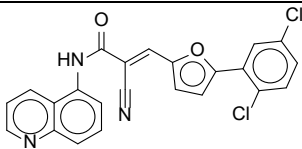
\*Values in parentheses are for highest-resolution shell. Each dataset was derived from a single crystal.

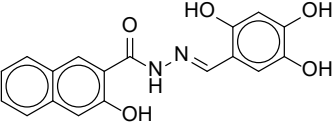
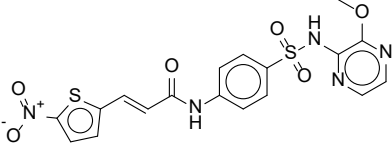
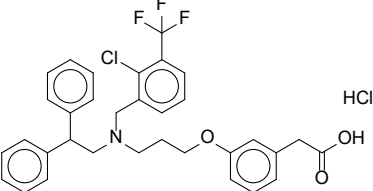
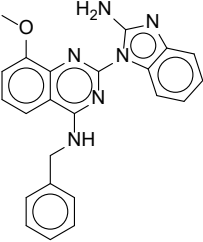
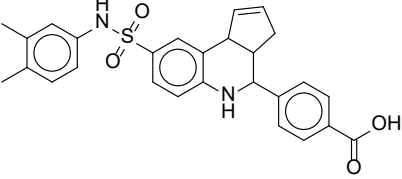
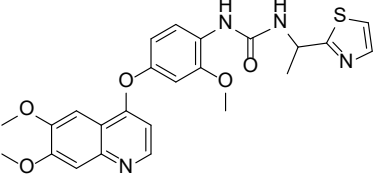
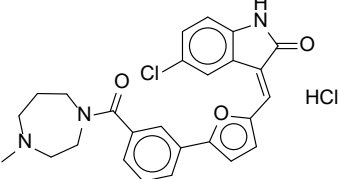
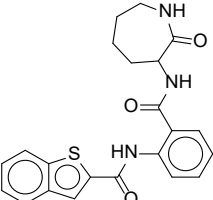
Substrate	$K_M$ ( $\mu\text{M}$ )	$k_{\text{cat}}$ ( $\text{min}^{-1}$ )	$k_{\text{cat}}/K_M$ ( $\text{min}^{-1} \mu\text{M}^{-1}$ )	Relative rate
$\{^3\text{H}\}$ UDP-GlcNAc	$2.3 \pm 0.4$	$0.29 \pm 0.01$	$0.12 \pm 0.01$	6.7
UDP-GlcN-BODIPY	$2.9 \pm 0.3$	$0.052 \pm 0.002$	$0.018 \pm 0.002$	1

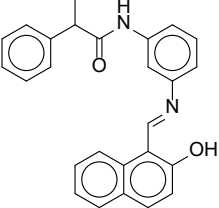
**Table S2:** Comparison of Michaelis-Menten kinetic parameters obtained for fluorescent OGT substrate **2** relative to UDP-GlcNAc using an oligopeptide acceptor in a radioactivity-based assay. Values represent the mean  $\pm$  S.E.M of triplicate values. Reactions were carried out in the presence of saturating concentrations of glycosyl acceptor ( $>10$ -fold above  $K_M$ ). Reactions using  $^3\text{H}$ -UDP-GlcNAc were previously performed by Lazarus *et al.*<sup>[3]</sup>

Peptide	Sequence	$K_M$ ( $\mu\text{M}$ )	$k_{\text{cat}}$ ( $\text{min}^{-1}$ )	$k_{\text{cat}}/K_M$ ( $\text{min}^{-1} \mu\text{M}^{-1}$ )	Relative rate
CKII	YPGGSTPV <b>SS</b> ANMM	$6.2 \pm 0.6$	$0.068 \pm 0.002$	$0.011 \pm 0.001$	1
TAB-1	PVSV <b>PYSS</b> AQSTS	$5.6 \pm 0.5$	$0.078 \pm 0.002$	$0.014 \pm 0.001$	1.3
HCF-1	VRVCSN <b>PPCS</b> THETGTTNTATTAT	$9.2 \pm 1.7$	$2.2 \pm 0.2$	$0.24 \pm 0.05$	21

**Table S3:** Michaelis-Menten kinetic parameters for OGT-catalyzed glycosylation of various peptide acceptors. Values represent the mean  $\pm$  S.E.M of triplicate values. Reactions were carried out in the presence of saturating concentrations of fluorescent glycosyl donor ( $>10$ -fold above  $K_M$ ). Residues in bolded red font indicate site of glycosylation.

Compound Name	Structure	Inhibition assay result
GW0742		$\text{IC}_{50}$ 13 $\mu\text{M}$ Hill slope -2.1
AGK2		$\text{IC}_{50} > 100 \mu\text{M}$

Dyngo-4a		IC <sub>50</sub> 7.1 μM Hill slope -0.9
Necro-sulfonamide		IC <sub>50</sub> 27 μM Hill slope -0.9
GW3965		IC <sub>50</sub> 12 μM Hill slope -2.4
ML240		IC <sub>50</sub> > 100 μM
MX69		IC <sub>50</sub> > 100 μM
Ki20227		IC <sub>50</sub> 44 μM Hill slope -4.5
CX-6258		IC <sub>50</sub> 35 μM Hill slope -0.9
ANA-12		IC <sub>50</sub> > 100 μM

Salermide		$IC_{50} > 100 \mu M$
-----------	---	-----------------------

**Table S4:** Summary of 11 hit compounds identified as OGT inhibitors from HTS that were re-ordered for follow up experiments. All compounds were obtained as dry powders from TargetMol Corp. (Wellesley Hills, MA). Compounds were triaged by first determining  $IC_{50}$  values against OGT in the presence of 0.02% Triton X-100. Five compounds did not show inhibition with re-ordered material and were discarded. Six compounds showed concentration-dependent inhibition and were carried forward for testing.

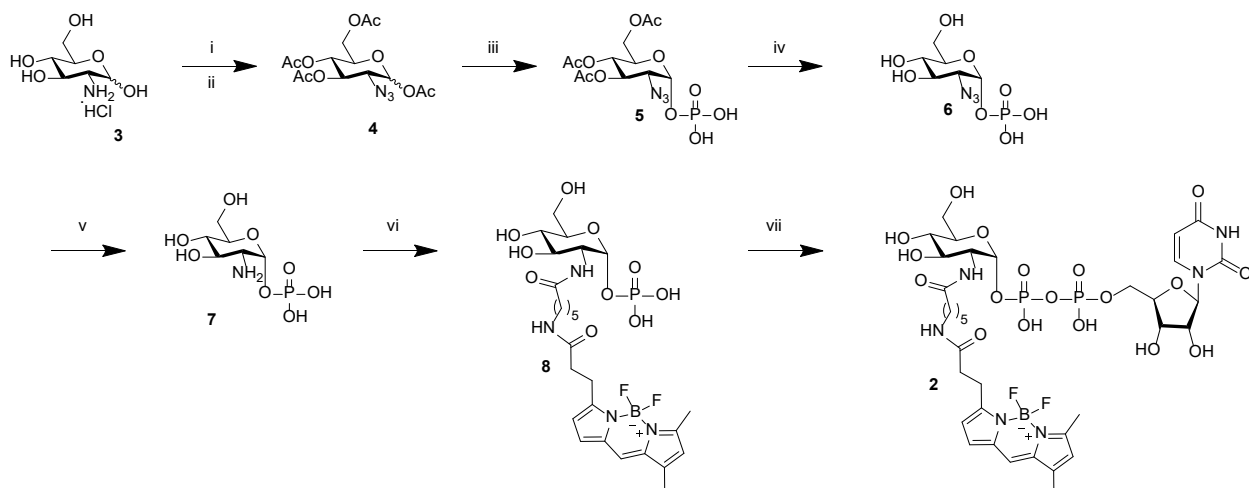
## SUPPLEMENTAL METHODS

### General Synthetic Procedures

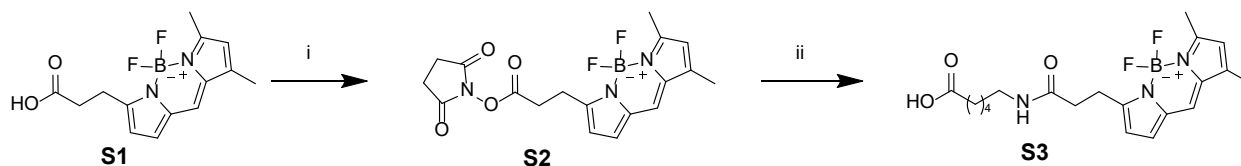
All synthetic reagents used in this study were obtained from Sigma-Aldrich (Oakville, ON), Carbosynth (San Diego, CA) or Alfa Aesar (Ward Hill, MA). Anhydrous reactions were carried out in flame-dried glassware under a positive pressure of dry argon. Air- or moisture-sensitive reagents and anhydrous solvents were transferred with oven-dried syringes or cannulae. Flash chromatography was performed using E. Merck silica gel (230-400 mesh). Solution-phase reactions were monitored using analytical thin layer chromatography (TLC) with E. Merck 0.2 mm pre-coated silica gel aluminium plates 60 F254; compounds were visualized by illumination with short-wavelength (254 nm) ultraviolet light and/or staining with ceric ammonium molybdate or potassium permanganate staining solution. Pyridine was dried extensively over activated 4 Å molecular sieves under argon. Custom synthesis of oligopeptides used for activity assays was carried out by Biomatik Corporation (Cambridge, ON, Canada) at >95% purity. <sup>1</sup>H NMR (600 MHz) and <sup>13</sup>C NMR (151 MHz) spectra were recorded at ambient temperature on a Bruker Avance II 600 spectrometer equipped with a 5 mm QNP cryoprobe. <sup>1</sup>H NMR spectra at 500 MHz and <sup>13</sup>C NMR spectra at 125 MHz were recorded at ambient temperature on a Bruker Avance III 500 spectrometer equipped with a 5mm TXI inverse ATM probe and BACS-60 robotic sample changer. Deuterated chloroform (CDCl<sub>3</sub>), dimethyl sulfoxide (DMSO-*d*<sub>6</sub>), methanol (CD<sub>3</sub>OD) or water (D<sub>2</sub>O) were used as NMR solvents. Chemical shifts are reported in ppm downfield from tetramethylsilane (TMS) and corrected using the solvent residual signal as a reference. Splitting patterns are designated as follows: s, singlet; d, doublet; t, triplet; q, quartet; p, pentet; hex, hextet; m, multiplet and br, broad.

### High Pressure Liquid Chromatography and Mass Spectrometry

Samples were analyzed and purified using an Agilent 1200 HPLC equipped with an Agilent 300SB-C18 column (9.4 × 250 mm, 5µ particle size). Compounds were eluted on the column at a flow rate of 2 mL/min using HPLC grade water and acetonitrile with 0.1% trifluoroacetic acid, or 50 mM aqueous ammonium acetate and methanol as the mobile phase. High-resolution mass spectrometry was performed using a Bruker maXis Impact UltraHigh-Resolution Quadrupole Time-of-Flight (UHR-QTOF) mass spectrometer using a gradient consisting of HPLC grade water and acetonitrile containing 0.1% formic acid at a flow rate of 0.3-0.5 ml/min. Ions were sprayed in positive mode with a voltage of 4200 V. Nitrogen drying gas was 180°C at a flow rate of 8 L/min. Data was acquired over a mass range of 300-2500 atomic mass units.



**Scheme S1:** Synthetic route towards UDP-GlcN-BODIPY (**2**). Reagents and conditions: i) imidazole-1-sulfonyl azide  $\cdot$ HCl,  $\text{CuSO}_4 \cdot 5\text{H}_2\text{O}$ ,  $\text{K}_2\text{CO}_3$ , MeOH, 2 h, 92%; ii)  $\text{Ac}_2\text{O}$ , pyridine, 10 h, 98%; iii)  $\text{H}_3\text{PO}_4$  (s), vacuum,  $60^\circ\text{C}$ , 44%; iv) NaOMe, MeOH, 92%; v)  $\text{H}_2$ , Pd/C, MeOH, 98%; vi) Cpd **10**, HBTU, DIPEA, DMF, 37%; vii) UMP-morpholidate, N-methylimidazole  $\cdot$ HCl, DMF, 45%.



**Scheme S2:** Synthetic route towards BODIPY-FL caproic acid. Reagents and conditions: i) DCC, NHS, DMF, 75%; ii) Caproic acid, DIPEA, DMF, 91%.

### 3,4,6-Tri-O-acetyl-2-azido-2-deoxy- $\alpha$ -D-glucopyranosyl phosphate (**5**)

Crystalline phosphoric acid (1.9 g, 19.5 mmol) was added to a flame-dried 500 mL round bottom flask under an argon atmosphere. 0.9 g (2.4 mmol) of tetra-O-acetyl-2-azido-2-deoxy-D-glucopyranose (**4**) was added, and the mixture was heated to  $60^\circ\text{C}$  in a sand bath under vacuum for 4 hours. The mixture was then cooled to room temperature and dissolved in 12 mL anhydrous THF. The solution was further cooled in an ice bath and then quenched with concentrated aqueous ammonium hydroxide (2 mL) until a pH of 7 was reached. The ammonium phosphate precipitate was removed by filtration and the filtrate was concentrated under reduced pressure. The crude product was purified by flash column chromatography (10:3:1 to 10:6:1 EtOAc:MeOH: $\text{H}_2\text{O}$ ) to give **5** as a brown solid (0.43 g, 44%). Spectral data were in agreement with previous reports<sup>[4]</sup>.  $^1\text{H}$  NMR (500 MHz, MeOD):  $\delta$  (ppm) 5.70 (dd,  $J = 2.4, 6.8$  Hz, 1H),

5.47 (dd,  $J = 9.8, 9.8$  Hz, 1H), 5.08 (dd,  $J = 9.8, 9.8$  Hz, 1H), 4.33 (d,  $J = 10.5$  Hz, 2H), 4.12 (m, 1H), 3.60 (d,  $J = 10.4$  Hz, 1H), 2.05 (s, 1H), 2.03 (s, 1H), 2.00 (s, 1H).

#### *2-Azido-2-deoxy- $\alpha$ -D-glucofuranosyl phosphate (6)*

3,4,6-Tri-O-acetyl-2-azido-2-deoxy- $\alpha$ -D-glucofuranosyl phosphate (**5**) (0.43 g, 1.05 mol) was dissolved in anhydrous methanol (10 mL) in a 50 mL round bottom flask. A spatula tip of NaOMe (100 mg, 0.002 mol) was added to the solution, which was stirred at room temperature overnight. The mixture was acidified with Amberlite IR-120 ion exchange resin ( $H^+$  form) until a pH of 7 was reached. The solution was then filtered and concentrated under reduced pressure to yield **6** as a brown solid, which was carried forward without further purification (0.36 g, 92%). Spectral data were in agreement with previous reports<sup>[4]</sup>.  $^1H$  NMR (500 MHz, MeOD):  $\delta$  (ppm) 5.56 (d,  $J = 3.4$  Hz, 1H), 3.99-3.84 (m, 3H), 3.64 (m, 2H), 3.21 (d,  $J = 10.4$  Hz, 1H).

#### *2-Amino-2-deoxy- $\alpha$ -D-glucofuranosyl phosphate (7)*

Compound **6** (235 mg, 0.83 mmol) was added to a 100 mL round bottom flask. Palladium hydroxide on carbon (23 mg, 0.16 mmol), water (10 mL) and methanol (10 mL) were added, and the flask was charged with an atmosphere of hydrogen. The suspension was stirred vigorously for 2 hours at room temperature and was then filtered and washed with methanol (20 mL). The filtrate was concentrated under reduced pressure to yield **7** as an amorphous solid (215 mg, 92%).  $^1H$  NMR (500 MHz,  $D_2O$ )  $\delta$  5.51 (dd,  $J = 7.6, 3.3$  Hz, 1H), 3.94 (ddd,  $J = 10.1, 5.1, 2.3$  Hz, 1H), 3.87 (dd,  $J = 12.3, 2.3$  Hz, 1H), 3.80 – 3.72 (m, 2H), 3.42 (dd,  $J = 10.1, 9.2$  Hz, 1H), 2.99 (ddd,  $J = 10.3, 3.4, 1.8$  Hz, 1H).  $^{13}C$  NMR (126 MHz,  $D_2O$ )  $\delta$  92.73, 72.41, 71.95, 69.98, 60.86, 55.11. HRMS (ESI<sup>-</sup>) Calculated 258.0378, found 258.0337 [M-H]<sup>-</sup>.

#### *2-deoxy-2-N-[6-((4,4-difluoro-5,7-dimethyl-4-bora-3a,4a-diaza-s-indacene-3-propionyl)amino)hexanoyl]- $\alpha$ -D-glucofuranosyl phosphate (8)*

To a 100 mL flame dried round bottom flask under an argon atmosphere was added compound **7** (106 mg, 0.35 mmol), BODIPY-FL-X-OH (**S3**) (60 mg, 0.15 mmol) and DMF (50 mL). HATU (60 mg, 0.22 mmol) and triethylamine (140  $\mu$ L, 1 mmol) were added, and the suspension was stirred vigorously overnight at room temperature. The mixture was then concentrated by co-evaporation with toluene (3 x 50 mL) and was purified directly using flash column chromatography (10:3:1 to 10:60:1

EtOAc:MeOH:H<sub>2</sub>O) to yield compound **8** as a red crystalline solid (38 mg, 37%). <sup>1</sup>H NMR (500 MHz, Methanol-d<sub>4</sub>) δ 7.44 (s, 1H), 7.02 (d, *J* = 4.0 Hz, 1H), 6.33 (d, *J* = 4.0 Hz, 1H), 6.21 (s, 1H), 5.44 (dd, *J* = 7.0, 3.4 Hz, 1H), 3.96 (dt, *J* = 10.6, 2.9 Hz, 1H), 3.92 – 3.81 (m, 2H), 3.73 – 3.63 (m, 2H), 3.36 (t, *J* = 9.4 Hz, 1H), 3.23-3.17 (m, 4H), 2.61 (t, *J* = 7.5 Hz, 2H), 2.51 (s, 3H), 2.28 (d, *J* = 7.5 Hz, 2H), 2.27 (s, 3H), 1.64 (dd, *J* = 9.3, 6.1 Hz, 2H), 1.54 – 1.45 (m, 2H), 1.36 (dd, *J* = 7.9, 7.7 Hz, 2H). <sup>13</sup>C NMR (151 MHz, D<sub>2</sub>O) δ 181.45, 177.39, 174.65, 161.42, 155.61, 146.42, 135.30, 133.11, 128.71, 124.79, 120.97, 116.71, 93.01, 72.16, 71.27, 70.16, 60.71, 53.94, 39.15, 35.60, 27.97, 25.53, 24.94, 24.35, 14.18, 10.50. HRMS (ESI<sup>+</sup>) Calculated 647.2464, found 647.2471 [M+H]<sup>+</sup>.

### *Synthesis of UDP-GlcN-BODIPY (2)*

To a 50 mL flame dried round bottom flask under argon was added compound **8** (32 mg, 0.05 mmol), Uridine 5'-monophosphomorpholidate 4-morpholine-N,N'-dicyclohexylcarboxamidinium salt (68 mg, 1 mmol), and *N*-methylimidazolium HCl (31 mg, 0.26 mmol) in 5 mL DMF. The solution was stirred overnight, concentrated under reduced pressure, and then purified on an Agilent 1200 series HPLC equipped with an Agilent XDB-C18 Eclipse reversed-phase column (9.4 × 250 mm, 5 μ particle size). Mobile phase conditions: 50:50 to 70:30 A:B over 20 minutes, 2 mL/min flow rate, solvent A = 50 mM NH<sub>4</sub>OAc, solvent B = MeOH, product retention time 17.2 min. The collected material was lyophilized to give **2** as a red powder (21 mg, 45%). For long-term storage, the product was kept as a dry powder at -20°C in a vial which was protected from light. <sup>1</sup>H NMR (600 MHz, Deuterium Oxide) δ 7.84 (d, *J* = 8.1 Hz, 1H), 7.31 (s, 1H), 6.98 (d, *J* = 4.0 Hz, 1H), 6.28 (d, *J* = 4.0 Hz, 1H), 6.20 (s, 1H), 5.82 (d, *J* = 4.4 Hz, 1H), 5.80 (d, *J* = 8.1 Hz, 1H), 5.48 (dd, *J* = 7.0, 3.3 Hz, 1H), 4.29 (dd, *J* = 9.0, 5.0 Hz, 1H), 4.26 (dd, *J* = 9.0, 5.0 Hz, 1H), 4.22 – 4.18 (m, 2H), 4.16 – 4.13 (m, 1H), 3.98 (dt, *J* = 10.5, 3.0 Hz, 1H), 3.93 (ddd, *J* = 10.1, 4.7, 2.3 Hz, 1H), 3.86 (dd, *J* = 12.5, 2.3 Hz, 1H), 3.79 – 3.73 (m, 2H), 3.51 (dd, *J* = 10.1, 9.1 Hz, 1H), 3.13 (t, *J* = 6.6 Hz, 2H), 3.11 (t, *J* = 7.3 Hz, 2H), 2.61 (t, *J* = 7.3 Hz, 2H), 2.44 (s, 3H), 2.29 (t, *J* = 7.6 Hz, 2H), 2.17 (s, 3H), 1.53 (p, *J* = 7.6 Hz, 2H), 1.42 (p, *J* = 7.5 Hz, 2H), 1.25 – 1.16 (m, 2H). <sup>13</sup>C NMR (151 MHz, D<sub>2</sub>O) δ 179.98, 177.48, 174.72, 165.94, 151.46, 141.38, 133.13, 128.82, 124.83, 120.91, 116.68, 102.30, 94.69, 88.66, 82.95, 73.94, 73.01, 70.94, 69.68, 69.39, 60.40, 53.56, 39.15, 35.53, 34.77, 28.00, 25.62, 24.96, 24.34, 22.38, 14.19, 10.54. HRMS (ESI<sup>-</sup>) Calculated 951.2567, found 951.2573 [M-H]<sup>-</sup>.



### *Synthesis of BODIPY-FL N-hydroxysuccinimidyl ester (S2)*

BODIPY-FL (175 mg, 0.6 mmol), *N*-hydroxysuccinimide (275 mg, 2.4 mmol), and dicyclohexylcarbodiimide (495 mg, 2.4 mmol) were added to a 25 mL flame-dried round bottom flask under an argon atmosphere. Anhydrous dimethylformamide (6 mL) was added and the mixture was stirred at room temperature for 3 hours. When the reaction was judged complete by TLC, the solvent was removed by co-evaporation with toluene and 10 mL EtOAc was added to the flask. The mixture was then filtered and the filtrate was purified by flash column chromatography (99:1 DCM:MeOH) to yield **S2** as a red amorphous solid (220 mg, 75%). <sup>1</sup>H NMR (500 MHz, Chloroform-*d*) δ 7.09 (s, 1H), 6.88 (d, *J* = 4.0 Hz, 1H), 6.33 (d, *J* = 4.0 Hz, 1H), 6.12 (s, 1H), 3.38 (t, *J* = 7.3 Hz, 2H), 3.08 (t, *J* = 7.4 Hz, 2H), 2.83 (br s, 4H), 2.56 (s, 3H), 2.25 (s, 3H). HRMS (ESI<sup>+</sup>) Calculated 412.1256, found 412.1252 [M+Na]<sup>+</sup>.

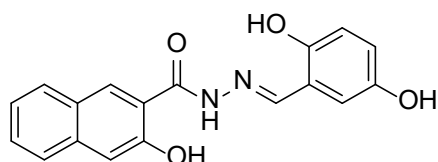
### *Synthesis of BODIPY-FL Caproic acid (S3)*

To a flame-dried 50 mL round bottom flask was added compound **S2** (220 mg, 0.57 mmol), caproic acid (150 mg, 1.14 mmol), and anhydrous DMF (5 mL). Diisopropylethylamine (0.2 mL, 1.14 mmol) was added, and the solution was stirred at room temperature for 3 hours. The solvent was removed under reduced pressure and the materials were dissolved in 10 mL MeOH. Amberlite IR-120 (H<sup>+</sup> form, 50 mg) was added and the mixture was stirred for 10 min until a pH of ~7 was reached. The mixture was then filtered, concentrated, and purified by flash column chromatography (0.5% to 10% MeOH in DCM) to yield **S3** as a red amorphous solid (220 mg, 96%). <sup>1</sup>H NMR (500 MHz, Methanol-*d*<sub>4</sub>) δ 7.43 (s, 1H), 7.01 (d, *J* = 4.0 Hz, 1H), 6.32 (d, *J* = 4.0 Hz, 1H), 6.21 (s, 1H), 3.22 (t, *J* = 7.6 Hz, 2H), 3.19 – 3.15 (m, 2H), 2.60 (t, *J* = 7.6 Hz, 2H), 2.51 (s, 3H), 2.30-2.26 (m, 5H), 1.60 (p, *J* = 7.5 Hz, 2H), 1.49 (p, *J* = 7.1 Hz, 2H), 1.37 – 1.31 (m, 2H). <sup>13</sup>C NMR (126 MHz, MeOD) δ 174.53, 161.30, 158.52, 145.80, 136.50, 134.89, 129.59, 125.74, 121.32, 117.71, 40.25, 36.05, 30.74, 30.05, 27.50, 25.83, 25.67, 11.17. HRMS (ESI<sup>+</sup>) Calculated 428.1933, found 428.1931 [M+Na]<sup>+</sup>.

### Synthesis of Dyngo-4a (9)

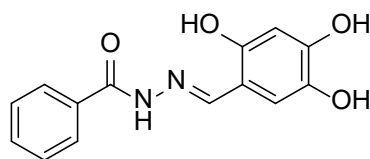
Dyngo-4a was synthesized as previously reported<sup>[5]</sup>. Characterization data were in agreement with previous values.

### Synthesis of (*E*)-*N'*-(2,5-dihydroxybenzylidene)-3-hydroxy-2-naphthohydrazide (10)



To a solution of 3-hydroxy-2-naphthoic hydrazide (202.2 mg, 1.0 mmol) in EtOH (3 mL) was added 2,5-dihydroxybenzaldehyde (1.0 eq., 140.0 mg, 1.0 mmol). The reaction mixture was subjected to microwave irradiation for 20 min at 120°C. The reaction was allowed to cool, and the resulting precipitate collected. The precipitate was washed with chilled EtOH (2 × 4 mL) and chilled Et<sub>2</sub>O (1 × 4 mL) to afford the title compound as a pale yellow-green solid (295 mg, 92%); m.p. >270°C (decomp.). *N*-acylhydrazone compounds exist as *syn*- and *anti-periplanar* conformers about the amide CO-NH bond in solution<sup>[6]</sup>. This conformational isomerism is evident in the <sup>1</sup>H NMR spectrum for the title compound. Data corresponding to the major conformer is reported below. <sup>1</sup>H NMR (400 MHz, DMSO-*d*<sub>6</sub>) δ 12.08 (br. s, 1H), 11.35 (br. s, 1H), 10.35 (s, 1H), 9.02 (s, 1H), 8.61 (s, 1H), 8.47 (s, 1H), 7.91 (d, *J* = 8.2 Hz, 1H), 7.77 (d, *J* = 8.2 Hz, 1H), 7.52 (dd, *J* = 8.2, 7.5 Hz, 1H), 7.38 – 7.33 (m, 2H), 7.03 (d, *J* = 2.1 Hz, 1H), 6.83 – 6.72 (m, 2H); <sup>13</sup>C NMR (101 MHz, DMSO-*d*<sub>6</sub>) δ 163.6, 154.1, 150.2, 149.8, 148.1, 135.8, 130.2, 128.6, 128.2, 126.7, 125.8, 123.8, 119.8, 119.2, 118.9, 117.1, 113.6, 110.5; LRMS (ESI<sup>-</sup>) *m/z* (%): 321 (100) (*M*-H), HRMS (ESI<sup>-</sup>) *m/z* calculated for C<sub>18</sub>H<sub>13</sub>N<sub>2</sub>O<sub>4</sub> (*M*-H) 321.0875; found 321.0903.

### Synthesis of (*E*)-*N'*-(2,4,5-trihydroxybenzylidene)benzohydrazide (11)



To a solution of benzohydrazide (149.8 mg, 1.1 mmol) in EtOH (3 mL) was added 2,4,5-trihydroxybenzaldehyde (1.1 eq., 180.0 mg, 1.2 mmol). The reaction mixture was subjected to microwave irradiation for 30 min at 120°C. The reaction was allowed to cool, and the resulting precipitate collected. The precipitate was washed with chilled EtOH (2 × 4 mL) and chilled Et<sub>2</sub>O (1 × 4 mL) to afford

the title compound as a pale yellow solid (232 mg, 77%); m.p. >215°C (decomp.). <sup>1</sup>H NMR (400 MHz, DMSO-*d*<sub>6</sub>) δ 11.80 (s, 1H), 10.63 (s, 1H), 9.56 (s, 1H), 8.56 (s, 1H), 8.45 (s, 1H), 7.91 (d, *J* = 7.2 Hz, 2H), 7.61 – 7.50 (m, 3H), 6.88 (s, 1H), 6.34 (s, 1H); <sup>13</sup>C NMR (101 MHz, DMSO-*d*<sub>6</sub>) δ 162.4, 151.9, 149.3, 148.6, 138.5, 133.2, 131.7, 128.5 (2 × C), 127.5 (2 × C), 114.7, 109.5, 103.5; LRMS (ESI<sup>+</sup>) *m/z* (%): 273 (100) (*M*+H).

### Full-length OGT expression and purification

The plasmid containing the gene encoding full-length human OGT in a previously-reported pET28a vector<sup>[7]</sup> was transformed into competent *Escherichia coli* BL21 (DE3) cells (Invitrogen). Successful transformants were cultured in Terrific Broth supplemented with 50 µg/mL kanamycin at 37°C until an optical density of 1.8 absorbance units was reached. Protein expression was induced with 0.2 mM isopropyl β-D-thiogalactoside at 16°C for 18 h. Cells were harvested and resuspended in 2 mL BugBuster protein extraction reagent (EMD Millipore) per gram of cell pellet in the presence of 1 mg/mL lysozyme, 0.2 mg/mL DNase and an EDTA-free protease inhibitor tablet (Roche). The mixture was gently rocked at 4°C for 30 min and then clarified by centrifugation for 2 x 30 min at 18,000 x *g*. The cell lysate was then applied to a 1 mL HisTrap nickel column (GE Healthcare) which was pre-equilibrated in 50 mM HEPES, 500 mM NaCl and 1 mM DTT at pH 7.5. The protein was purified using an imidazole gradient of 20-500 mM over 50 min on an AKTA FPLC (GE Healthcare). Fractions judged as pure were pooled and dialyzed at 4 °C in 50 mM HEPES buffer containing 500 mM NaCl and 1 mM DTT at pH 7.4. Aliquots of OGT were flash frozen and stored at -80°C for future use.

### Truncated OGT expression and purification

OGT4.5 was expressed in *Escherichia coli* BL21 (DE3) cells and purified as previously described with a few minor changes<sup>[3]</sup>. Cells were grown to an OD<sub>600</sub> of between 1-1.2 in TB media before being cooled to 16°C for 30 min. Cells were then induced with 0.2 mM IPTG before shaking incubation overnight at 16°C. Cultures were pelleted at 5400 x *g*, and the pellets were resuspended in buffer A (20 mM Tris pH 7.4, 150 mM NaCl, and 40 mM imidazole), lysozyme, DNase 1, and 1 mM AEBSF. Cells were lysed by a cell disruptor, before being clarified by centrifugation at 41700 x *g*. Resulting supernatant was loaded onto a 5 ml HisTrap FF column (GE Healthcare), washed with buffer A, and then eluted with a stepwise gradient of buffer B (20 mM Tris 7.4, 150 mM NaCl, and 400 mM imidazole) in buffer A. Fractions containing protein were pooled and supplemented with THP to a final concentration of 1 mM. Cleavage of the His-

tag was achieved through incubation with HRV 3C protease at a ratio of 1 µg protease:100 µg protein overnight at 4°C. The protein sample was then diluted with 20 mM Tris pH 7.4 to a final concentration of 15 mM NaCl before being passed over a 5 ml HisTrap FF column (GE Healthcare) and a 5 ml HiTrap Q HP column (GE Healthcare). Elution was achieved with a stepwise gradient of 20 mM Tris pH 8.0 through to 20mM Tris pH 8 and 1M NaCl. Fractions containing protein were pooled, concentrated using Vivaspin® spin-concentrators (Sartorius) and size excluded on a Superdex 200 column (GE Healthcare) in 20 mM Tris pH 8.0 and 150 mM NaCl. Monodispersed fractions containing protein were collected, supplemented with THP to a final concentration of 1 mM, concentrated and snap frozen.

### **Crystallisation and structure determination**

Crystals were grown at 20°C using the sitting drop technique with 2 µL of protein/ligand mix and 1 µL of reservoir. OGT4.5 (7 mg ml<sup>-1</sup>) was incubated with UDP (1 mM) for 1 hour, followed by HCF-1<sub>11-26</sub> peptide (3 mM) for 3 hours. Crystals were obtained in 1.45 M potassium sodium tartrate and 0.1 M Tris pH 8.5, similar to those previously reported<sup>[8]</sup>. Crystals were soaked with 750 µM substrate **2**, 1 mM MgCl<sub>2</sub> and 7.5 U of calf intestinal alkaline phosphatase in mother liquor for 4 hours. Crystals were cryo-protected in mother liquor supplemented with 27% xylitol and flash cooled. Diffraction data was collected at the Diamond Light Source in Oxford, UK on beamline I04-1. Data reduction and processing was completed through the *DIALS* pipeline<sup>[9]</sup>. A previously obtained OGT4.5 structure (4n39) was used as a search model for molecular replacement through PHASER<sup>[8]</sup>. Model building and refinement consisted of multiple cycles of manual adjustments in COOT<sup>[10]</sup> and refinement in REFMAC5<sup>[11]</sup>. Geometric restraints for substrate **2** were generated through AceDRG<sup>[12]</sup>. Structure figures were produced with Chimera<sup>[13]</sup> and Pymol<sup>[14]</sup>.

### **Fluorescent OGT activity assay**

Assays performed manually for assay development or enzyme characterization carried out in black Nunc 96- or 384-well microplates (cat. # 237108 or 262260, Thermo Fisher Scientific, Mississauga, ON). All reported concentrations represent final assay conditions unless otherwise specified. Microplates are typically centrifuged at 300 x g for 1 min after addition of reagents. In a typical 384-well experiment, a master mix containing various concentrations of fluorescent substrate **7c** and biotinylated peptide acceptor is made up in PBS containing 12.5 mM MgCl<sub>2</sub> and 1 mM DTT at pH 7.2. The reaction is commenced by the addition of recombinant OGT PBS to a final well volume of 25 µL and final OGT concentration of 20-200 nM. The plate is then incubated at ambient temperature for up to 60 min, during

which time the reaction rate was shown to be linear (Figure S15). The reaction is terminated by the addition of 25  $\mu$ L stop mix containing 7.5 mM UDP and 0.2 mg/mL streptavidin-coated magnetic beads (Trilink Technologies M-1002). The plate is incubated at room temperature for at least 30 min to allow for streptavidin-biotin binding, and is then subjected to an automated washing procedure using a BioTek EL406 plate washer containing a magnetic adapter and a BioTek 384F magnet (12 wash cycles, 100  $\mu$ L PBS dispensed per well, 6 mm aspiration height offset, 4 min initial resting time on magnet, 1 min rest between washes). At the end of the wash cycle, a final dispense of 50  $\mu$ L PBS per well is performed using the syringe dispenser of the BioTek washer. The fluorescence signal is read using a Biotek Neo2 multimode plate reader using 490nm excitation and 525 nm emission wavelengths. Each well is read using an area scan function which records the mean signal of 9 individual scans in a grid pattern with 1.0 micron spacing between each point. Data were analyzed and plotted using GraphPad Prism 5.

### ***In vitro* OGT inhibition assays**

IC<sub>50</sub> experiments were carried out using the general procedure for the OGT activity assay, with the following modifications. Inhibitor stocks in DMSO were diluted to various concentrations and were pre-incubated with recombinant OGT on ice for at least 15 minutes. The reaction was commenced by addition of a master mix containing both donor and acceptor substrates at their respective  $K_M$  values. Reactions proceeded at room temperature for < 60 min, during which the reaction progress was shown to be linear (Figure S15). The % relative activity of OGT in the presence of inhibitor was assessed by normalizing fluorescent signal against controls which contained only DMSO (100% activity) and controls which contained 2 mM UDP (0% activity). % activities were plotted as a function of log<sub>10</sub> concentration of inhibitor. Curves were fitted using a sigmoidal 4-parameter log(inhibitor) vs response function in GraphPad Prism 5; IC<sub>50</sub> values were calculated from the inflection point of sigmoidal curves. Full  $K_i$  inhibition experiments were carried out in a similar manner, except that the concentration of substrate was varied to at least 5-fold above and 5-fold below the  $K_{M(app)}$  in the presence of varying concentrations of inhibitor.  $K_i$  values were calculated using the non-linear regression function of GraphPad Prism 5.

### **Automated High-Throughput Screening**

Optimization and validation of the OGT activity was performed to ensure suitability for HTS using conditions identical to those implemented during screening. Signal-to-background ratio, Z'-scores, DMSO tolerance to 2%, and linearity of reaction profiles were assessed in 384-well plates (Nunc; cat. # 262260). Assays were run under balanced conditions<sup>[15]</sup> wherein concentrations of donor and acceptor substrates

at their  $K_{M (app)}$  values were used in the presence of 20 nM recombinant OGT. Buffer used for screening consisted of PBS at pH 7.2 supplemented with 12.5 mM  $MgCl_2$ , 1 mM DTT and 0.01% Triton X-100. Library compounds were tested at a final concentration of 100  $\mu$ M (DMSO 1% final concentration). Automated HTS was carried out using Momentum laboratory automation workflow software equipped with a Spinnaker BenchTrack 4-axis microplate robot (Thermo Fisher Scientific, Mississauga, ON). Solutions of substrate and enzyme were dispensed with a Multidrop Combi (Thermo Fisher Scientific) to a final volume of 25  $\mu$ L. Compounds were added to assay plates using a 384-well pin tool equipped with slotted 200 nL pins (FP3NS200, V&P Scientific) and a Freedom EVO 100 (TeCan, Morrisville, NC) liquid handling system which was calibrated to transfer 250 nL of 10 mM compound stocks in 100% DMSO. Plates were centrifuged at 300 x  $g$  for 20 seconds after dispensing and were then incubated at room temperature for 60 min. Reactions were stopped by addition of 25  $\mu$ L stop solution described above using the peristaltic pump dispenser equipped with a 5  $\mu$ L cassette of an EL406 combination washer/dispenser (BioTek, Winooski, VT). Plates were incubated for a further 30 minutes at room temperature and then subjected to an automated wash cycle and fluorescence detection as described previously. Z'-scores for each plate were calculated from the mean % response of the control population and standard deviation of the control population according to equation (1). Data from plates which showed Z'-scores  $\geq 0.5$  were retained for analysis and hit confirmation. The hit selection cutoff for inhibitors was set as 3 standard deviations from the % activities of the uninhibited controls. Hit confirmation in triplicate was carried out using identical conditions as primary screening. Hit population and distribution was visualized using GraphPad Prism 5. Hits were triaged computationally using the PAINS and Toxicophore filters using the online service FAFDrugs-4<sup>[16]</sup>.

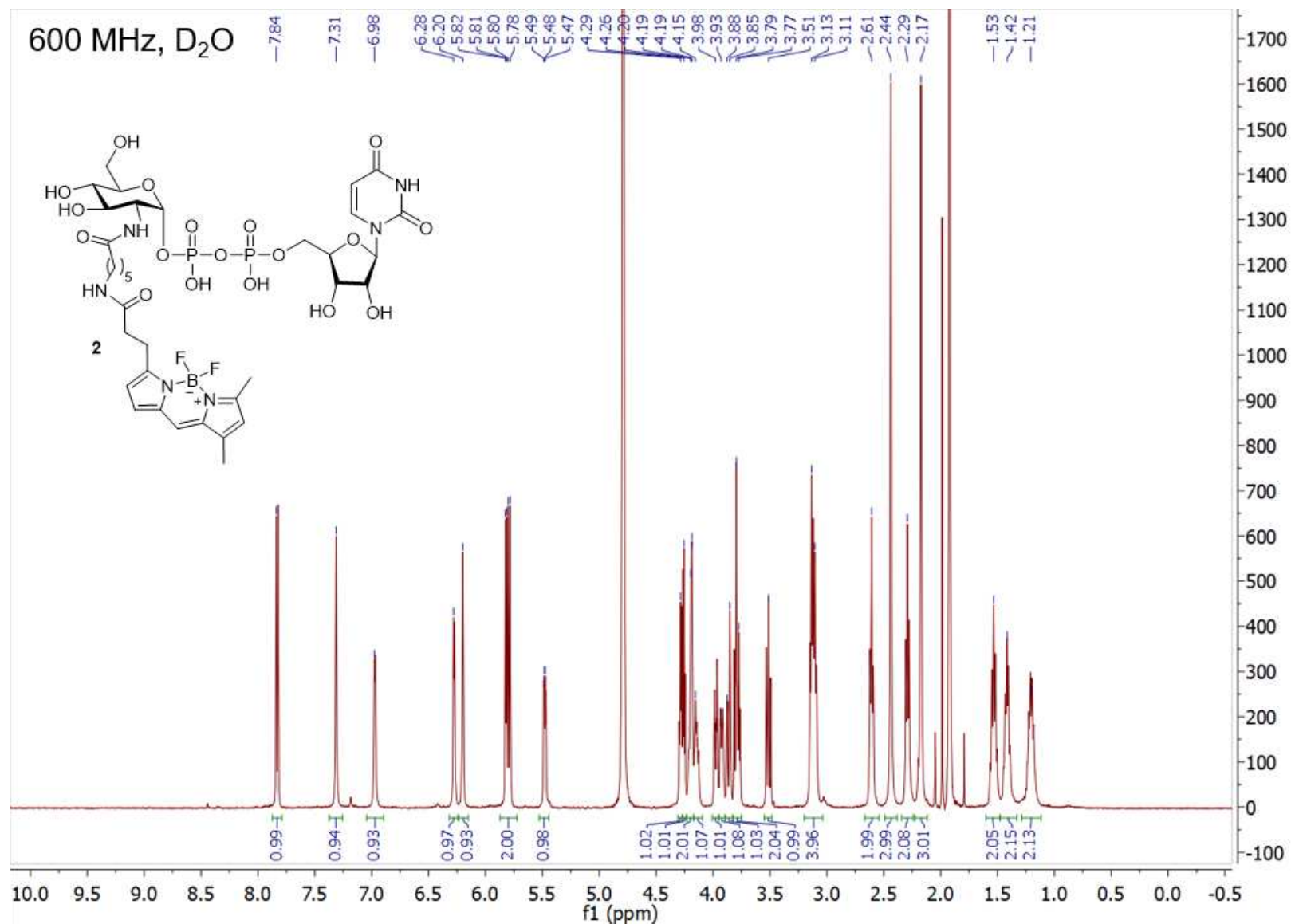
### **Differential Scanning Fluorimetry**

Differential Scanning Fluorimetry was performed using an Applied Biosystems QuantStudio 3 RT-PCR machine equipped with a 96-well heating block. Reactions were performed in MicroAmp 96-well optical PCR plates (Applied Biosystems) at a final volume of 20  $\mu$ L per well. Reactions contained 0.6 mg/mL protein, 1X Protein Thermal Shift Dye (Thermo Fisher Scientific) and 0.2- 100  $\mu$ M final concentration of ligand in 1X PBS. Reaction components were made up on ice; thermal shift assays were carried out at temperatures ranging from 25 to 95°C at a ramp rate of 0.05°C/sec. Fluorescence measurements were taken using a 580 nm excitation / 623 nm emission filter set. Reactions were performed in triplicate and data were analyzed using QuantStudio Design and Analysis software and GraphPad Prism 5. Melt curves were fitted to a Boltzmann sigmoidal curve and apparent  $T_m$  values were determined by calculating the inflection point of the fitted curves.

### ***In vitro* dynamin activity assay**

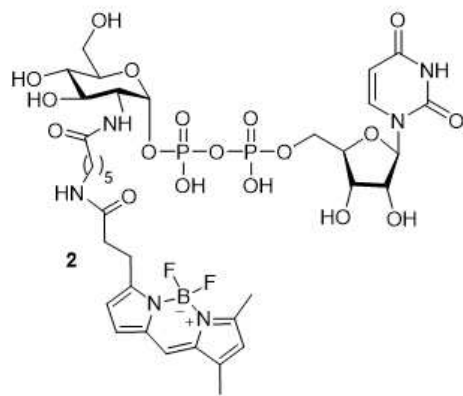
Dynamin GTPase activity (and the impact of small molecule inhibitors; 0-100  $\mu$ M) was measured *in vitro* using an adaptation of the Malachite Green phosphate detection absorbance-based assay within a 96-well plate format as described previously<sup>[17]</sup>. Dynamin solution (30  $\mu$ L) was added to reaction buffer mixture (120  $\mu$ L) to yield a final reaction of: 150  $\mu$ L well volume, 20 nM recombinant full length human dynlba, 11 mM Tris-HCl, 30 mM NaCl, 150  $\mu$ M GTP, 4  $\mu$ g/mL PS liposomes, 1.6 mM MgCl<sub>2</sub>, 0.06% Tween-80, 0.1  $\mu$ M AEBSF, 1  $\mu$ g/mL leupeptin, pH 7.4. Salt-adjusted buffer, basal dynamin and drug alone controls were included with each experiment to make the relevant absorbance subtractions. Plates were then incubated at 37°C for 30 min with shaking at 800 rpm. The assay was stopped, by sequestering magnesium ions, using 0.5 M EDTA (10  $\mu$ L) followed by the addition of Malachite Green solution (40  $\mu$ L; 2% (w/v) ammonium molybdate tetrahydrate, 0.15% (w/v) Malachite Green, 4 M HCl) to react with free inorganic phosphate. The absorbance (650 nm) was measured and raw data exported to Microsoft Excel and GraphPad Prism for further analysis and generation of inhibition curves/coefficients.

# <sup>1</sup>H and <sup>13</sup>C NMR Spectra of Compound 2

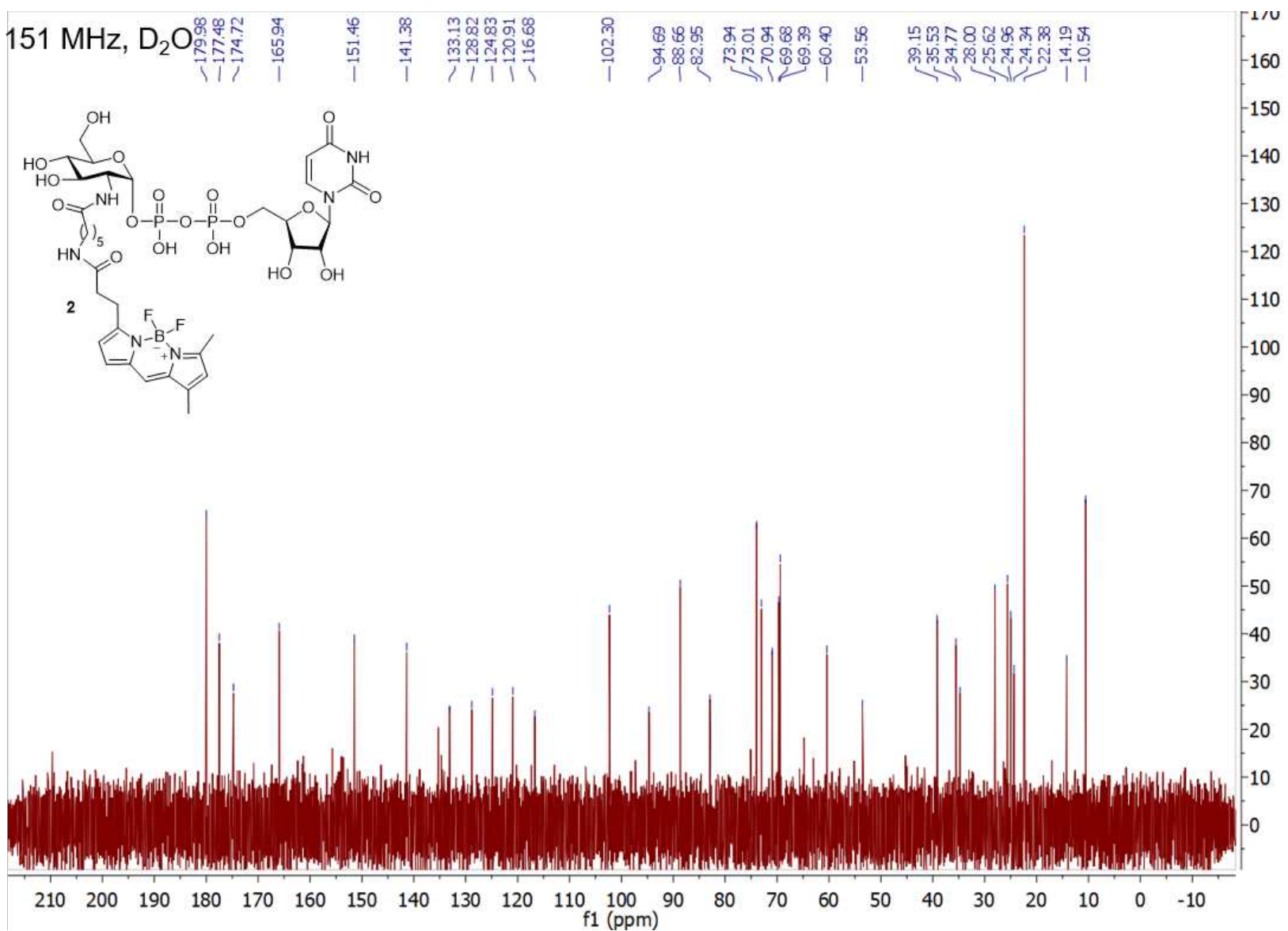




151 MHz, D<sub>2</sub>O



- 179.98
- 177.48
- 174.72
- 165.94
- 151.46
- 141.38
- 133.13
- 128.82
- 124.83
- 120.91
- 116.68
- 102.30
- 94.69
- 88.66
- 82.95
- 73.94
- 73.01
- 70.94
- 69.68
- 69.39
- 60.40
- 53.56
- 39.15
- 35.53
- 34.77
- 28.00
- 25.62
- 24.96
- 24.34
- 22.38
- 14.19
- 10.54



## Supplemental References

- [1] J. D. Hirsch, L. Eslamizar, B. J. Filanoski, N. Malekzadeh, R. P. Haugland, J. M. Beechem, R. P. Haugland, *Anal. Biochem.* **2002**, *308*, 343–357.
- [2] J.-H. Zhang, *J. Biomol. Screen.* **1999**, *4*, 67–73.
- [3] M. B. Lazarus, Y. Nam, J. Jiang, P. Sliz, S. Walker, *Nature* **2011**, *469*, 564–569.
- [4] S. Masuko, S. Bera, D. E. Green, M. Weiwer, J. Liu, P. L. Deangelis, R. J. Linhardt, *J. Org. Chem.* **2012**, *77*, 1449–1456.
- [5] A. McCluskey, J. A. Daniel, G. Hadzic, N. Chau, E. L. Clayton, A. Mariana, A. Whiting, N. N. Gorgani, J. Lloyd, A. Quan, et al., *Traffic* **2013**, *14*, 1272–1289.
- [6] A. B. Lopes, E. Miguez, A. E. Kümmerle, V. M. Rumjanek, C. A. M. Fraga, E. J. Barreiro, *Molecules* **2013**, *18*, 11683–11704.
- [7] C. Martinez-Fleites, M. S. Macauley, Y. He, D. L. Shen, D. J. Vocadlo, G. J. Davies, *Nat. Struct. Mol. Biol.* **2008**, *15*, 764–765.
- [8] M. B. Lazarus, J. Jiang, V. Kapuria, T. Bhuiyan, J. Janetzko, W. F. Zandberg, D. J. Vocadlo, W. Herr, S. Walker, *Science (80- )*. **2013**, *342*, 1235–1239.
- [9] G. Winter, D. G. Waterman, J. M. Parkhurst, A. S. Brewster, R. J. Gildea, M. Gerstel, L. Fuentes-Montero, M. Vollmar, T. Michels-Clark, I. D. Young, et al., *Acta Crystallogr. Sect. D Struct. Biol.* **2018**, *74*, 85–97.
- [10] P. Emsley, K. Cowtan, *Acta Crystallogr. Sect. D Biol. Crystallogr.* **2004**, *60*, 2126–2132.
- [11] G. N. Murshudov, P. Skubák, A. A. Lebedev, N. S. Pannu, R. A. Steiner, R. A. Nicholls, M. D. Winn, F. Long, A. A. Vagin, *Acta Crystallogr. Sect. D Biol. Crystallogr.* **2011**, *67*, 355–367.
- [12] F. Long, R. A. Nicholls, P. Emsley, S. Gražulis, A. Merkys, A. Vaitkus, G. N. Murshudov, *Acta Crystallogr. Sect. D Struct. Biol.* **2017**, *73*, 112–122.
- [13] E. F. Pettersen, T. D. Goddard, C. C. Huang, G. S. Couch, D. M. Greenblatt, E. C. Meng, T. E. Ferrin, *J. Comput. Chem.* **2004**, *25*, 1605–1612.
- [14] Schrodinger LLC, “The PyMOL Molecular Graphics System,” can be found under [www.pymol.org](http://www.pymol.org), **n.d.**
- [15] J. Yang, R. A. Copeland, Z. Lai, *J. Biomol. Screen.* **2009**, *14*, 111–120.
- [16] D. Lagorce, L. Bouslama, J. Becot, M. A. Miteva, B. O. Villoutreix, *Bioinformatics* **2017**, *33*, 3658–3660.
- [17] A. Quan, P. J. Robinson, *Methods Enzymol.* **2005**, *404*, 556–569.